eman ta zabal zazu

Universidad
del País Vasco

Euskal Herriko
Unibertsitatea

NMR studies of the interactions of glycan antigens with monoclonal antibodies

Ilaria Calloni

Doctoral Thesis

2020

Universidad del País Vasco
Euskal Herriko Unibertsitatea

NMR studies of the interactions of glycan antigens with monoclonal antibodies

Ilaria Calloni

Doctoral Thesis

2020

Supervisors:

Prof. Dr. Jesús Jiménez Barbero
Dr. Niels-Christian Reichardt

University Tutor: Prof. Dr. Nuria Sotomayor Anduiza (UPV/EHU)

This doctoral thesis has been performed at the Center for Cooperative Research in Biosciences (CIC bioGUNE).

CIC bioGUNE gsk
CENTER FOR COOPERATIVE RESEARCH IN BIOSCIENCES

A papà

__Acknowledgements__

Un grazie va' alla mia famiglia, ci siete sempre stati.

A Orny, Vale e Vale perchè siete casa. A Simo e Silvia, amiche di una vita. A Laura e Fra per i gin tonic e perché questa esperienza è cominciata con voi. Un ultimo, ma non meno importate ringraziamento va' al Prof. Francesco Nicotra e alla Prof. Laura Cipolla, perché la curiosità e l'amore per la ricerca è nata grazie a voi, nei corridoi dell'U3.

Conflict of interest

MenAfrivac is a trademark of the Serum Institute of India; Nimenrix is a trademark of Pfizer; Menactra is a trademark of Sanofi-Pasteur; Menveo is atrademark of GSK group of companies.

Contents

<u>Abbreviations</u>

^{1}H-^{13}C-HSQC: ^{1}H-^{13}C - Heteronuclear Single Quantum Coherence spectroscopy

AMBER: Assisted Model Building with Energy Refinement

CPS: Capsular polysaccharide

GAFF: General Amber Force Field

Gal: Galactose

GBS: Group B *Streptococcus*

gg: *gauche-gauche*

Glc: Glucose

GlcNAc: N-acetylglucosamine

gt: *gauche-trans*

Men: *Neisseria meningitidis*

mAb: monoclonal Antibody

MD: Molecular Dynamics

MenNAc: Mannosamine

Neu5Ac = NeuNAc: N-acetylneuramidic acid or commonly, Sialic acid

NMR: Nuclear Magnetic Resonance

NOE: Nuclear Overhauser Effect

NOESY: Nuclear Overhauser Effect SpectroscopY

QM: Quantum Mechanics

ROE: Rotating frame NOE

RoG: Radius of gyration

STD: Saturation Transfer Difference

tg: *trans-gauche*

TOCSY: Total Correlation SpectroscopY

tr-NOESY: TRansferred Nuclear Overhauser Effect

Abstract

Carbohydrates (glycans, saccharides, sugars) are one of the most variable and complex molecules of biological systems. They are usually located at the cell membrane, mainly as glycoconjugates, glycoproteins or glycolipids and play an important role in the specific molecular recognitions of different entities, of different size and complexity, such as lectins, enzymes, virus, or antibodies. Within glycans, polysaccharide capsules (CPS) are universal structures found on the cell surface of a broad range of bacterial species. The polysaccharide capsule often constitutes the outermost layer of the cell; as such, it mediates the direct interactions between the bacterium and its immediate environment.

The knowledge of intermolecular communication, at atomic and molecular scale, between carbohydrates and their receptors should lead to the understanding and eventually the modulation of the biological signals involved in physiological and pathological events. Since structure and function are intrinsically correlated, the three-dimensional shape, dynamics and presentation of these molecules play a role in the recognition processes.

In this work, we have employed a variety of Nuclear Magnetic Resonance spectroscopy (NMR) techniques, assisted by different computational approaches, in particular Molecular Dynamics (MD) simulation and *ab initio* methods, for obtaining atomic-scale information on the conformation, dynamics and interactions, in solution, of different types of capsular polysaccharides present in *Neisseria meningitis* and *Streptococcus B*.

Chapter I

The introduction of this thesis is focused on the carbohydrates, the general characteristics of these molecules and the forces that govern their preferential conformations in solution. The chapter concludes with a description of the experimental methods that have been employed in this thesis to elucidate the structure and interactions of polysaccharides.

Chapter II

In this chapter, after a brief introduction on *Neisseria meningitis*, we have discussed in detail the molecular structures and dynamics features of Men A, X, C, W and Y. We have applied a combination of NMR spectroscopy, Molecular Dynamics simulations (MD) and quantum mechanics studies to define the preferred conformations of these molecules around the different glycosidic linkages and the three-dimensional shape of the entire polysaccharide. For Men A, some glycomimetics have been studied and compared. Additionally, for Men C, W and Y, the role of acetylation at diverse hydroxyl groups has also been investigated. Moreover, the molecular recognition features of the interactions of Men C and W with their specific mAbs have also been explored to determine the ligand epitope.

Chapter III

In this chapter, after a brief introduction on *Streptococcus B*, the three-dimensional structures and dynamics characteristics of the GBS Ia, Ib, II, III, IV and V natural polysaccharides have been unraveled, by employing a combination of NMR methods and MD simulations. The conformations and dynamics of GBS Ia and Ib, which present a very similar chemical composition have been compared. For GBS III, the role of the sialic acid in maintaining the three-dimensional structure and the molecular recognition features with their specific mAbs has also been elucidated.

__Resumen__

Los hidratos de carbono (glicanos, sacáridos, azúcares) son probablemente las moléculas más variables y complejas de los sistemas biológicos. Por lo general, se encuentran en la membrana celular, principalmente como glicoconjugados, glicoproteínas o glicolípidos y juegan un papel importante en el reconocimiento molecular específico de diferentes entidades, como lectinas, enzimas, virus o anticuerpos. Dentro de los glicanos, las polisacáridos de la cápsula (CPS) son estructuras universales que se encuentran en la superficie celular de una amplia gama de especies bacterianas. A menudo, constituyen la capa más externa de la célula y como tal, median las interacciones directas entre la bacteria y su entorno inmediato.

El conocimiento de la comunicación intermolecular, a nivel atómico y molecular, entre los carbohidratos y sus receptores, debería conducir a la comprensión y a la modulación de las señales biológicas involucradas en eventos fisiológicos y patológicos. Dado que la estructura y la función están intrínsecamente correlacionadas, la forma tridimensional, la dinámica y la presentación de estas moléculas juegan un papel esencial en los procesos de reconocimiento.

En este trabajo, hemos empleado una variedad de técnicas de espectroscopía de Resonancia Magnética Nuclear (NMR), asistidas por diferentes métodos computacionales, en particular simulaciones de Dinámica Molecular (MD) y métodos *ab initio*, para obtener información, a nivel atómico, sobre la conformación, la dinámica y las interacciones, en solución, de diferentes tipos de CPS presentes en *Neisseria meningitis* y *Streptococcus B*.

Capítulo I

La introducción de esta tesis se centra en los carbohidratos, las características generales de estas moléculas y las fuerzas que gobiernan sus conformaciones en solución. El capítulo concluye con una descripción de los métodos experimentales que se han empleado en esta tesis para dilucidar la estructura y las interacciones de los polisacáridos.

Capítulo II

En este capítulo, después de una breve introducción sobre *N. meningitis*, hemos discutido en detalle las estructuras moleculares y las características dinámicas de Men A, X, C, W e Y. Hemos aplicado una combinación de espectroscopía de RMN, simulaciones de Dinámica Molecular (DM) y estudios de mecánica cuántica para definir las conformaciones de estas moléculas alrededor de los diferentes enlaces glicosídicos y la forma tridimensional del polisacárido. En particular, para Men A, se han estudiado y comparado algunos glicomiméticos. Además, para Men C, W e Y, se ha investigado el papel de la acetilación de los diversos grupos hidroxilo. Además, se han explorado las características de reconocimiento molecular de las interacciones de Men C y W con sus mAbs específicos, para determinar el epítopo del ligando.

Capítulo III

En este capítulo, después de una breve introducción sobre *Streptococcus B*, mediante el empleo de una combinación de métodos de RMN y simulaciones MD se han desvelado las estructuras tridimensionales y las características dinámicas de los CPS de GBS Ia, Ib, II, III, IV y V. Se han comparado las conformaciones y la dinámica de GBS Ia y Ib, que presentan una composición química muy similar. Para GBS III, también se ha dilucidado el papel del ácido siálico en el mantenimiento de la estructura tridimensional y las características de reconocimiento molecular con sus mAbs.

Chapter

1

General Introduction

1.1 Biological relevance of Carbohydrates

Carbohydrates (glycans, saccharides, sugars) are located in the cell membrane, mainly as glycoconjugates, glycoproteins or glycolipids and play an important role in the specific molecular recognitions of different entities, of different size and complexity, such as lectins, enzymes, virus, or antibodies.[1] Many important processes for life and disease are controlled by extracellular signals that are mediated by carbohydrates, including cell recognition, growth, apoptosis, and immune response (Fig 1.1.1). [2,3,4]
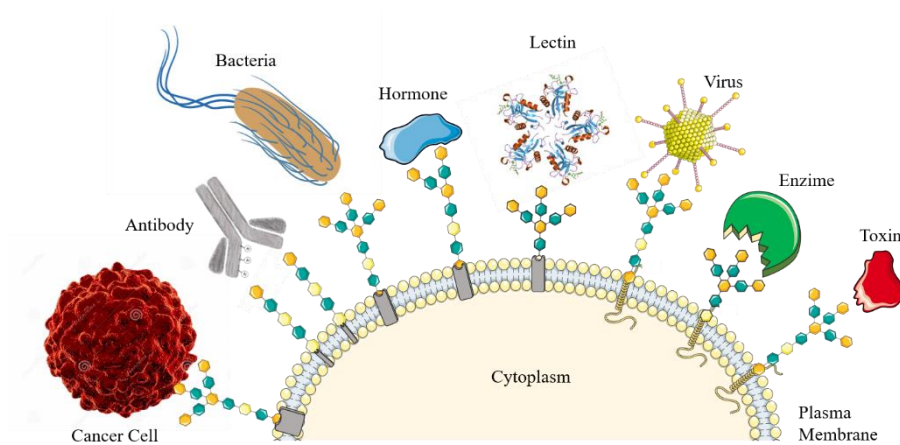
Figure 1.1.1 *Schematic view of the interactions of carbohydrates at the cell membrane.*

Within glycans, polysaccharide capsules are universal structures found on the cell surface of a broad range of bacterial species. The polysaccharide capsule often constitutes the outermost layer of the cell; as such, it mediates the direct interactions between the bacterium and its immediate environment. In fact, it is an important factor in the virulence of many animal and plant pathogens.[5,6,7]

Several possible functions for polysaccharide capsules have been suggested. In addition to playing a role promoting the adherence of bacteria to the host surfaces and to each other, by facilitating the formation of a biofilm and the colonization of various ecological niches,[8] they are also essential for the bacterial survival by

preventing desiccation.[9]   Moreover, the interactions between the capsular polysaccharide and the host's immune system can decide the outcome of the infection[10,11]. In the absence of specific antibodies, the presence of the capsule is thought to confer resistance to non-specific host defense mechanisms.

Capsular polysaccharides are composed of repeating single units (mono-saccharides) that are connected by glycosidic linkages.[12] They can be homo- or heteropolymers that may be additionally substituted at the hydroxyl groups by different functional groups (phosphate, sulfate,[13] acetyl[14]). They may be rather complex structures, including the possibility of branching.[15,16] Consequently, even a small number of monosaccharide components can lead to great structural diversity. Compared with the 4 bases of DNA and the 20 amino acids of proteins, more than 100 different monosaccharides and approximately 50 non-sugar components have been identified in bacterial polysaccharides.[17] All these characteristics increase the structural complexity of these molecules.

1.2 The conformation of carbohydrates

1.2.1 Monosaccharides

Monosaccharides are the building blocks of complex carbohydrates. The word "carbohydrate" means hydrate of carbon. Thus, a monosaccharide is formally composed by carbon atoms and water molecules. The high solubility of sugars is easily inferred; however, it would be incorrect to say that carbohydrates are exclusively hydrophilic molecules. Actually, the carbon chain, usually from five to seven carbon atoms, cyclizes to form rings of different size, e. g. the hexoses (six carbon atoms) can cyclize either to six-membered pyranose or to five-membered furanose rings (Fig. 1.2.1). Depending on the spatial orientation of each of the hydroxyl groups in the sugar ring, a highly polar and a less polar face of the molecule are defined. In fact, monosaccharides and, in general, carbohydrates are amphiphilic molecules, with a dual character. In other words, carbohydrates, even at the monosaccharide level, are water soluble molecules

that give rise to hydrophilic, as well as to hydrophobic interactions, with the right partner.
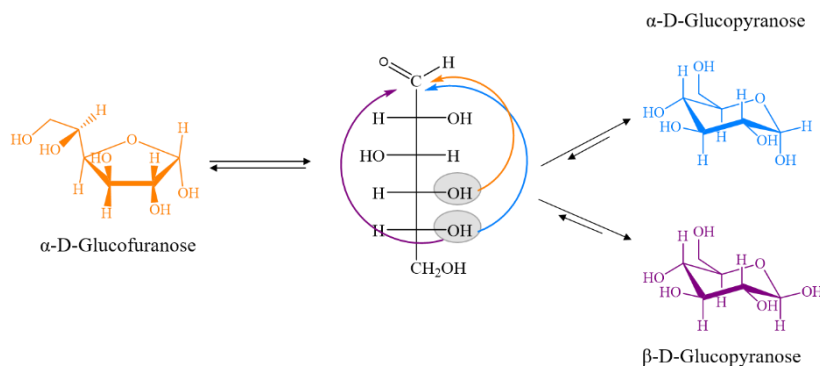
Figure 1.2.1 *Structural variability of a monosaccharide (glucose, Glc). Schematic representation of D-Glc in its open-chain form (fisher projection), α and β anomeric cyclic pyranose forms and β anomeric cyclic furanose form.*

The types of monosaccharides used for building up oligo- and poly-saccharides are not excessively large. The chemical difference between two types of sugars, e.g. Glucose (Glc) or Mannose (Man) or Galactose (Gal), is situated in the absolute configuration at each chiral center of the carbon backbone; by changing the configuration around a chiral carbon, a different sugar is obtained (Fig 1.2.2).
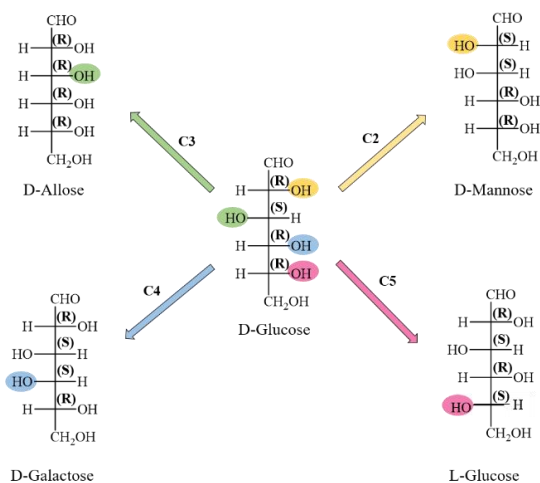
Figure 1.2.2 *Schematic representation of D-Glc and its epimers for the four chiral carbon atoms (Fischer representation). The absolute configuration is labeled with the (R) or (S) descriptors.*

During ring formation, due to the conversion of the planar sp^2-carbonyl carbon atom into a chiral tetrahedral sp^3 carbon, the glycosidic hydroxyl group can acquire two configurations, called α and β anomers (Fig 1.2.1). The difference is in the orientation of the hydroxyl group in the anomeric position (C1) that can be either axial (α) or equatorial (β) with respect to the plane of the sugar ring.

The six-membered ring usually display one of the two preferred conformations, the two-alternative low energy chair geometry showed in Fig 1.2.3. Depending on the substituents and their relative orientations (axial or equatorial), one of the two chairs is more stable. For example, for the β-D-Glc the most stable conformation is the $^4C_1$ chair conformation, adopted when all the hydroxyl groups are situated in equatorial position, since this 3D arrangement minimizes the steric clashes that characterize alternative the $^1C_4$ conformation. In this case, the 1,3-diaxial hydroxyl groups are oriented in the same direction, with the consequent steric and dipolar repulsion. [18]

$^4C_1$ $^1C_4$
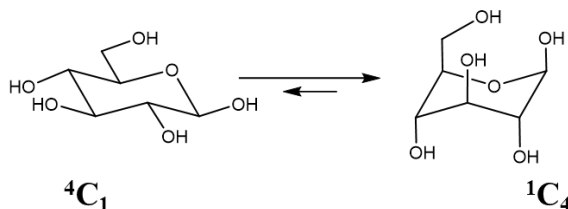
Figure 1.2.3 *Representation of $^4C_1$ and $^1C_4$ chairs geometry.*

The nomenclature is defined by placing a plane through C2, C3, C5 and O5 and looking the disposition of the C1 and C4 in relation to this (Fig 1.2.4). The interconversion between the two chairs is very complex and can be explained by the representation proposed by Cremer and Pople in 1975 (Fig 1.2.5).[19,20] They introduced three polar spherical coordinates, corresponding to the ring-puckering parameters to describe the nonplanar character of a closed ring. For six-membered ring the coordinates are: Q (amplitude), ϕ (phase) and θ (angle). The amplitude (Q) measure the deviation from planarity ring ($Q = 0$) and the phase angles (ϕ) describe the type of distortion. [21]
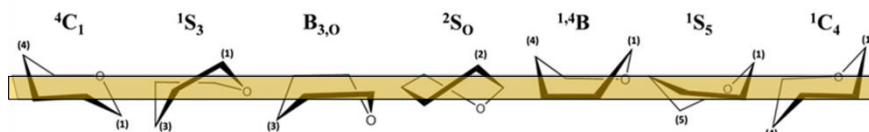
Figure 1.2.4 *Ring conformations adopted by monosaccharide rings. The first and the last one represent the energetically favored chair conformations: $^4C_1$ or $^1C_4$, depending on the position of carbons 1 and 4 (above or below the sugar ring plane, as noted by the position of the numeral).*
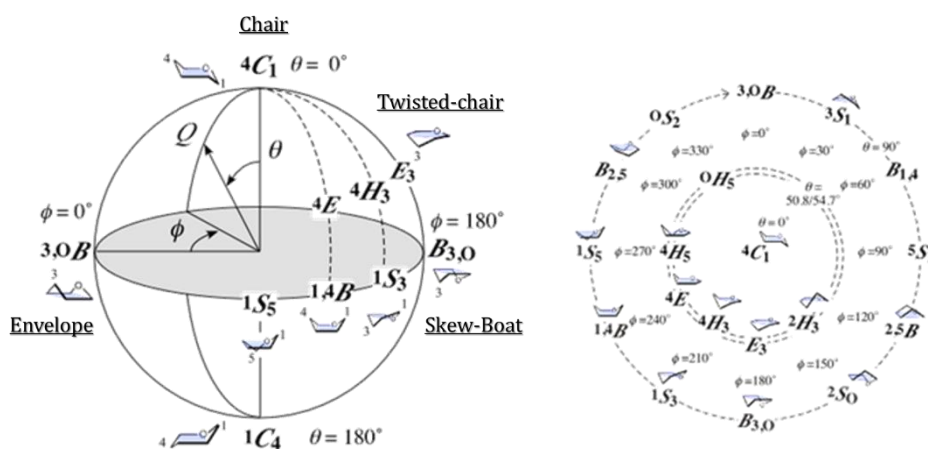
Figure 1.2.5 *Cremer-Pople representation of ring puckering* [20]

1.2.2 The glycosidic linkage

A disaccharide originates from the condensation reaction (glycosylation) [22,23,24] between two monosaccharides. The reaction involves the hydroxyl group at the anomeric position of one monosaccharide moiety (glycosyl donor) and one attachment point at the other monosaccharide (glycosyl acceptor), which can be any of the available hydroxyl groups, including the glycosidic function itself. Since the formed glycosidic bond can acquire two configurations, α and β, given

the availability of several attaching points, a glycosylation reaction can generate different disaccharides.

When two or more sugar residues are linked together in a sequence, new structural parameters have to be introduced. Figure 1.2.6a represents the three torsion angles that are required to define the relative orientation between the units of a model disaccharide: ϕ, ψ and ω. If the glycosidic linkage does not involve the position 6 of the *glycosyl acceptor*, only ϕ and ψ are required (Fig 1.2.6b).

The ϕ and ψ dihedral angles describe the orientation around the glycosidic linkages and they are defined as ϕ= H-C1-O-Cx and ψ= C1-O-Cx-Hx, where x is referred to the aglycon position. When the glycosidic linkage involves the position 6 of the aglycon, also the ω dihedral angle (ω=O5-C5-C6-O6) is required to define the spatial orientation of the molecule. Clearly, only some combinations of $\phi/\psi/\omega$ are favored from an energy view point.
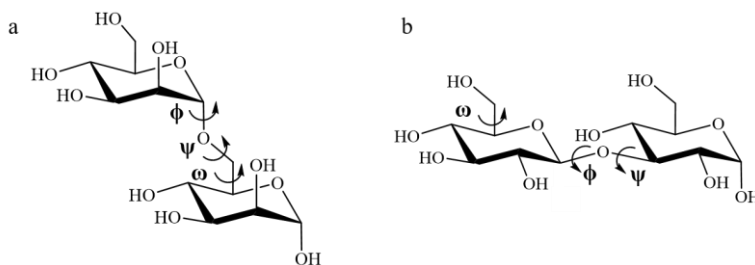
Figure 1.2.6 *(a) Representation of the torsion angles in αGlc1-6αGlc disaccharide; (b) representation of the torsion angles in αGlc1-4αGlc disaccharide.*

1.2.3 The Anomeric effect

The anomeric effect was initially defined as the preference for an electronegative substituent at the anomeric carbon to be in an axial rather than in an equatorial orientation.[25,26] In cyclohexane, it is well known that substituents attached to the ring tend to prefer the equatorial position over the axial one, due to unfavorable steric interactions for the axial conformer. However, contrary to steric predictions, electronegative substituents at the anomeric position of pyranose

sugars and other heterocycles were observed to adopt predominantly the axial orientation. This phenomenon was named as the anomeric effect.[27]

The preference for the axial conformation is attributed to the favorable interaction between a lone electron pair located in a molecular orbital (n) on either glycoside oxygen atoms and the vicinal anti-bonding molecular orbital (σ*). It is possible to distinguish between the *exo*-anomeric effect and the *endo*-anomeric effect.[28] The *endo*-anomeric effect arises from the favorable electronic interaction between the electron lone pair at the *endo*-cyclic O5 and the periplanar anti-bonding molecular orbital (σ*) of the C1-O1 bond. The donation of electron density from the ring oxygen is possible only if the acceptor empty molecular orbital is geometrically properly oriented. This is the case for α glycosides, but not for β glycosides. As a result, in α glycosides, the O5-C1 bond is slightly short when compared to the O5-C5 bond, because of its partial double bond character, while the C1-O1 bond is slightly longer (Fig 1.2.7).

endo-anomeric effect
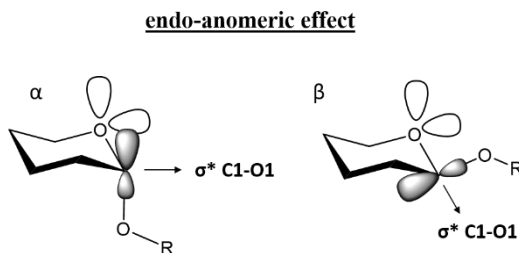
Figure 1.2.7 *Schematic representation of the lone pair-σ* interactions responsible for the endo-anomeric effects in α- and β- glycosides.*

In contrast, the *exo*-anomeric effect is common to both α and β glycosides. The anti-parallel arrangement of one lone pair on the *exo*-cyclic oxygen with respect to the anti-bonding O5-C1 bond may allow the electron back donation, thus stabilizing those conformations for which the values of ϕ are consistent with this geometric requirement. More precisely, this interaction is more favorable than the interaction of a lone pair orbital of the same oxygen with the C1-C2 σ*. This difference is attributed to the difference in polarization between the C1-O5 and C1-C2 bonds, producing a larger σ* orbital centered on the less electronegative

atom of the polarized bond. This remark is supported by the observation that the anomeric effect increases with the electronegativity of the substituent and decreases in solvents of high dielectric constant.[28] As result of the *exo*-anomeric effect, the C1-O1 bond is shorter than the other C-O bonds (Fig. 1.2.8).
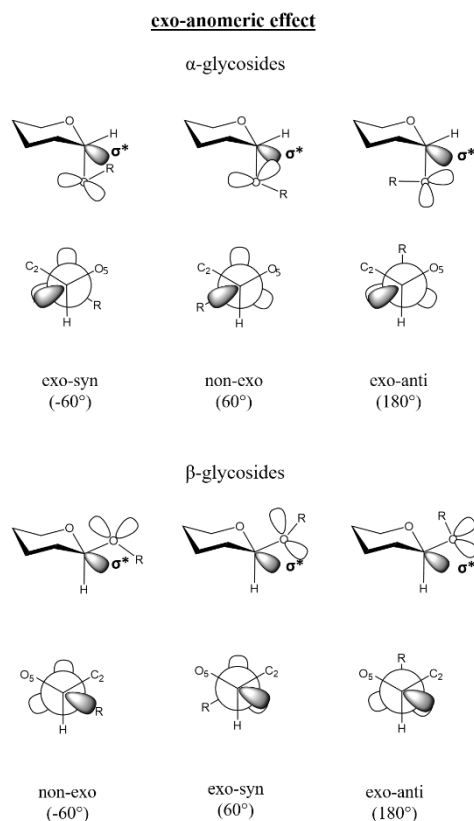
Figure 1.2.8 *Schematic representation of the lone pair-σ* interactions responsible for the exo-anomeric effects in α- and β- glycosides. The exo-syn conformation is the favorite.*

The combination of steric and electrostatic interactions generates the preference for two orientations of the glycosidic torsion, the *exo-syn*, ϕ (H1-C1-O1-Cx): -60º and +60º for the α and β forms.

1.2.4 The flexibility around C5-C6 bond

In monosaccharides with an exocyclic hydroxymethyl group there is three staggered situations around the O5-C5-C6-O6 dihedral angle (ω in Fig 1.2.6a) that can be considered. Fig. 1.2.9 shows the three different rotamers that this torsion angle can assume for α-Glc and α-Gal.
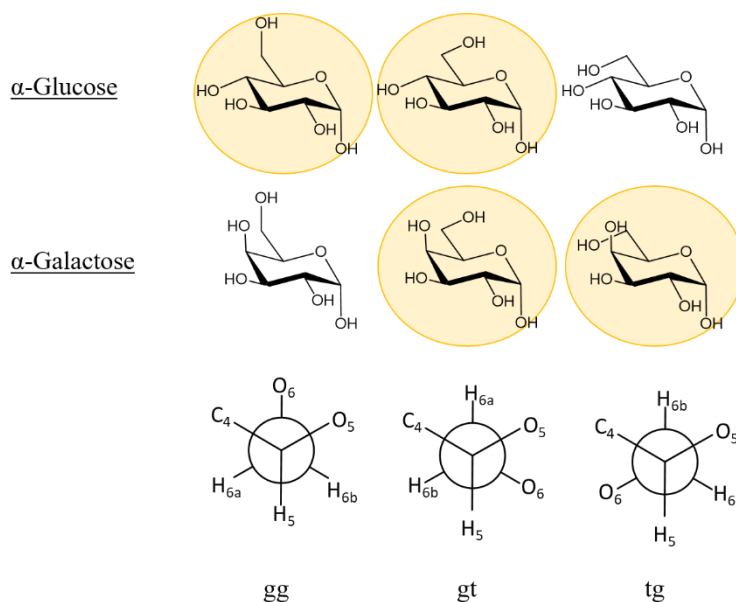
Figure 1.2.9 *(Above) The gg, gt and tg rotamers of α-Glc and α-Gal. The preferred conformations are highlighted in yellow. (Below) the possible rotamers around the C5-C6 bound, represented in the Newman projections.*

These three rotamers are called gg (gauche-gauche), gt (gauche-trans) and tg (trans-gauche) and correspond at -60°, 60° and 180° wherein O5 is the reference atom.

The driving force for the preference of any of these three conformations is based on the proper combination of steric, stereoelectronic and solvation effects. In particular, for Glc, the presence of the equatorial hydroxyl in position 4 makes the tg conformation unfavorable, due to a repulsion between O6 and O4, which would be close in this conformation. In the same manner, for Gal, the gg conformation is unfavorable. [29]

1.3 Conformational studies

The complexity of the study of the three-dimensional structure of carbohydrates derives from the high flexibility of these molecules and from the presence of different conformations that coexist in equilibrium in solution. The variability of the anomeric status, ring size and conformation, linkage position and number of residues represent a formidable issue for the study of glycan's conformations and dynamics.

Important progresses have been made possible by the spectacular improvements in the development and application of NMR[30] techniques in this field, also intimately bound to the advances in computational chemistry methods, from the available software to the new hardware technologies (GPU processors). Thus, the strategic combination of NMR methods with computational analysis, including Molecular Dynamics (MD) simulations and quantum mechanics (QM) *ab initio* techniques, has resulted in an increase in the understanding of the behavior of the carbohydrates in solution.[31,32,33]

1.3.1 Nuclear Magnetic Resonance: Basic concepts

Nuclear Magnetic Resonance (NMR)[34,35] is physical phenomenon that displays tremendous applications in chemical, biochemical, biological, and biomedical research. It allows studying diverse processes, from composition (chemical structure) and molecular dynamics (in different time scales) to interaction events. Moreover, it is a non-invasive and non-destructive technique.

NMR spectroscopy is related with the intrinsic property of those atomic nuclei that have a spin quantum number different to 0. Every nucleus displays an associated magnetic moment, **μ**, defined by **μ = γP**, where P is the angular moment and **γ** the magnetogyric ratio, which is characteristic of each nucleus. Both the angular momentum and the magnetic moment are vector quantities and show orientation and magnitude.

The magnitude and the orientation of the associated magnetic moment with the nuclear spin can only adopt a limited number of values. For a spin of magnetic quantum number n, there are 2n+1 possible angular moments, taking values from –n to +n. For example, for nuclei with spin number of n=½, like ^{1}H, ^{13}C, ^{15}N and ^{31}P, there are two possible spin states: m_s= +½ (α) and m_s= -½ (β).

In the absence of an external magnetic field, these levels are degenerated, both states have the same energy, and both are equally populated. However, in the presence of an external magnetic field (B_0), this degeneration disappears and the population is redistributed in favor of the lowest energy level, according to the Boltzmann law, as shown in Eq. 1.1

$$\frac{N_\alpha}{N_\beta} = e^{\frac{-\Delta E}{k \cdot T}}$$

Equation 1.1 *Where $N_{low/upp}$ is the spin state population distribution, k is the Boltzmann's constant, T the temperature and ΔE the energy difference between both momentum states.*

The difference between the two energy levels (Zeeman levels) is proportional to the applied magnetic field according to equation 1.2.

$$\Delta E = \gamma \, \hbar \, B_0$$

Equation 1.2 *Where ΔE is the energy difference between both momentum states, B_0 is the applied magnetic field, γ is the magnetogyric ratio, and ħ is the reduced Planck constant or Dirac constant. (Fig. 1.3.1).*
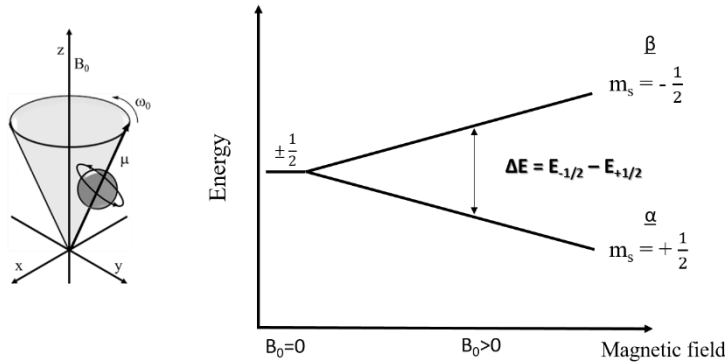
Figure 1.3.1 *(Left) representation of the precession motion; (right) splitting of the nuclei spin states in the presence of external magnetic field.*

The NMR signal results from the difference between the energy absorbed for the nuclear spins in the presence of a radiofrequency (*rf*). This generates a transition from the low energy state to the high energy state. When the system returns to the equilibrium, the energy emitted follows the inverse step, from the high-energy state to the low-energy state and the signal is produced.

Therefore, the NMR signal is proportional to the population difference between both states, which depends on the intensity of the applied magnetic field. Consequently, the use of high magnetic fields increases the sensitivity of the technique.

The magnetic moment of every nucleus precesses around the external magnetic field (B_0). The frequency of this precession is called *Larmor* resonance frequency (ω_0), which is different for each particular nucleus and is associated to the energy difference between both levels. The Larmor frequency depends on its magnetogyric constant γ and on the applied magnetic field intensity, B_0, and it is equivalent to the energy difference between the two spin levels (eq 1.3).

$$\omega_0 = \gamma B_0 = \Delta E / \hbar$$ **Eq. 1.3** *Where ω_0 is the Larmor frequency.*

However, there are small perturbations in the local magnetic field (B_i) associated with every nucleus, mainly due to the presence of the vicinal electrons, which produce shielding or deshielding on the resonance frequency (eq 1.4).

$$\omega_0 = \gamma\,(B_0 - B_i) \qquad\qquad \textbf{\textit{Eq. 1.4}}\ \textit{Where B_i is the local magnetic field.}$$

The result is that nuclei with different chemical environments precess with slightly different Larmor frequencies (chemical shift, δ, expressed in ppm), which permits to identify them, converting NMR in a very powerful structural characterization tool.

1.3.2 NMR and carbohydrates

NMR is one of the most commonly used techniques to characterize different molecular features of sugars thanks to its versatility. Recent advances in resolution and sensitivity[36] have allowed to gain access to robust procedures for achieving the determination of the structural, conformational, and dynamics of many complex oligosaccharides.[37,38,39,40] At the same time, NMR has become a powerful tool to monitor molecular interactions and to deduce atomic features of recognition processes at different levels of complexity.[41,42,43] It is important to remember that glycans are highly flexible molecules and precisely, this flexibility has important consequences on their three-dimensional structures and therefore, on the molecular recognition events they are involved.

All the NMR parameters display important information of saccharide structure, dynamics and interactions. Chemical shifts depend on the environment of the observed nucleus and therefore, they encode information on the relative configurations of the close stereocenters and the spatial proximity of the different sugar units in an oligosaccharide. Vicinal coupling constants, $^{3}J_{HH}$, are particularly useful to determine the relative orientation of the coupled nuclei through Karplus-like equations. Nuclear Overhauser enhancement spectroscopy (NOESY) provide semiquantitative information on the proximity of NMR-active

nuclei (usually protons) and therefore, the NOE is a key parameter for the conformational analyses around the glycosidic linkages. Relaxation-based techniques, as STD-NMR, allow identifying sugar-binders to receptors, as well as the glycan binding epitopes.

1.3.2.1 *J* coupling costants

After Raymond Lemieux empirical observations, Nobel Laureate Martin Karplus, described a relationship between the torsion angle established between vicinal hydrogens and the $^3J_{HH}$ coupling constant:[44,45]

$$^3J_{HH} = A + B cos\phi + C cos^2\phi$$

Equation 1.5 *Where φ is the dihedral angle between the two protons analyzed.*

Equation 1.5 provides the relationship between $^3J_{HH}$ and the dihedral angle between protons. The vicinal H-H couplings are maximal for 180° or 0° dihedral angles (anti or eclipsed relation results in optimal orbital overlap) and are close to zero for angles around 90° (Fig. 1.3.2). This simple relationship accurately applies only for unstrained hydrocarbon systems. Indeed, the presence of electronegative substituents and ring constrains cause important perturbations to the values predicted by this equation.

For this reason, coefficients A, B and C have been introduced to add values for each particular kind of molecule, atom, and substituent. In this regard, different *Karplus-like* relationships have been refined for use in conformational studies of saccharides, and also when the dihedral angle, and therefore the vicinal J coupling, involves other atoms besides H as C, N or P. [45]

$\phi = 0°$ $\phi = 60°$ $\phi = 90°$ $\phi = 180°$

$^3J = 7\text{-}11\text{Hz}$ $^3J = 2\text{-}5\text{Hz}$ $^3J = 0\text{-}2\text{Hz}$ $^3J = 8\text{-}15\text{Hz}$
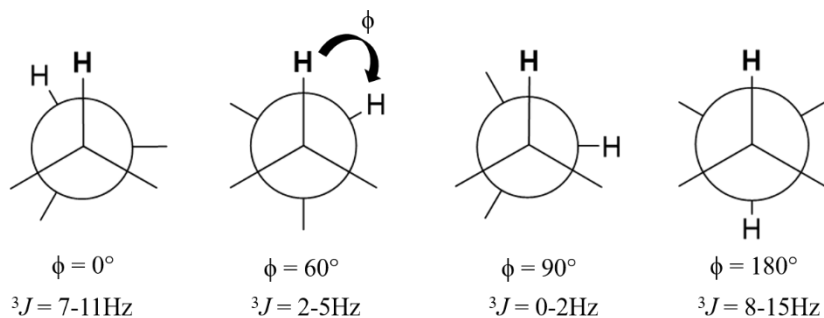
Figure 1.3.2 *Schematic representation of the possible rotamers and theoretical vicinal J coupling associated.*

In particular, in chapter II, we have made extensive use of *J* coupling analysis for the characterization of the conformation around an uncommon glycosidic linkage that involves a PO_3^- group.

Of note, scalar coupling constants have the advantage that the calculation of the expected average values over an ensemble of conformations is simple, allowing the characterization of the conformational equilibrium in terms of population distribution.[46]

Furthermore, not only $^3J_{HH}$ coupling constants, but also longer-range couplings ($^xJ_{HH}$, x > 3), as well as single and multiple-bond heteronuclear couplings[47] ($^xJ_{HY}$, $1 \leq x \leq 4$, and $Y = {}^{13}C, {}^{15}N, {}^{31}P...$) and homonuclear $^xJ_{YY}$ coupling constants provide information on the connectivity and geometric arrangements between nuclei.

In the absence of a specific and robust Karplus-like equation for a particular system is possible to use *ab initio* techniques to predict the theoretical J couplings around specific dihedral angles for different conformations and compare those to the experimental ones. [48]

1.3.2.2 The nuclear Overhauser effect (NOE)

The NOE is a key parameter for structural and conformational analysis of molecules due to its dependency on the internuclear (proton-proton) distances and motions.[49,50,51]

Relaxation is the process by which the equilibrium state of a spin is recovered after a perturbation. Recovery of the unperturbed distribution of population across the energy levels of a spin system is related to the cross-relaxation process. This event involves transitions between the different states of the system, whose spins are coupled through dipole-dipole interactions. The transitions affect to their populations and are reflected in a change on the intensity of the observed NMR signal. This change in the intensity of a given nuclei following perturbation of other one is the NOE. The change in intensity maybe positive (higher intensity in nucleus A after perturbation of nucleus B) or negative (lower intensity in nucleus A after perturbation of nucleus B). This phenomenological result is indeed related to molecular motion (rotational correlation time). For small molecules, with fast tumbling and short correlation times in the ps time scale, the NOE signals are positive. In contrast, large molecules, which display slowly tumbling in solution (long correlation times in the ns time scale), provide large and negative NOE signals.

Te relaxation theory behind these facts is tremendously complicated and will not be discussed herein since it is beyond the scope of this Thesis. However, it can be demonstrated that an efficient magnetic interaction between the magnetic dipoles of two nuclei (dipolar coupling) only takes place when they are very close in space. It is not necessary that the nuclei are connected by a chemical linkage. In fact, the efficiency of the interaction decreases with the sixth-power of the internuclear distance (Eq 1.6). Moreover, it also depends on the (averaged) relative orientations of the magnetic momentums of the spins, both between them and respect to the external magnetic field.

$$I_{NOE} \approx \langle 1/r^6 \rangle f(t_c)$$

Equation 1.6 *Where I_{NOE} is the NOE intensity, r is the proton-proton distance, and f is a function that depends also on the correlation time (t_c) that describes the motion of the interproton vector.*

This simple relationship can be employed to estimate distances from NOE values, following the so-called isolated spin pair approximation (ISPA). Thus, the experimental distances between two nuclei can be obtained relating the observed NOEs to the NOE values obtained for proton pairs that hold a fixed and known distance within the same molecule (Eq 1.7). The NOE is inversely proportional to the inverse of the sixth power of the distance between the interacting nuclei. In this case, knowing the NOE value between two nuclei (A-B) and the distance between them (Fig. 1.3.3), it is possible to calculate other distances corresponding to observed NOEs (A and C) in the same molecule through Eq 1.7.

$$\frac{\eta_{AB}}{\eta_{AC}} \cong \frac{\sigma_{AB}}{\sigma_{AC}} = \frac{r_{AB}^{-6}}{r_{AC}^{-6}}$$

Equation 1.7 Where η is the experimental intensities of the NOEs signals and r is the distance between the two protons.

This distance dependence reflects the necessity for the short-range dipolar interactions to originate the NOEs. In fact, at large distances the NOE effect is negligible, given the exponential decay of the NOE with increasing distances[52]. Depending on the molecular motion and the spectrometer frequency, the maximum distance which can be monitored in small oligosaccharides is *ca*. 4-5 Å, whereas for large molecules can go beyond 6 Å.

$$d_{AC} = \sqrt[6]{\frac{I_{AB}}{I_{AC}}} \cdot d_{AB}^6$$
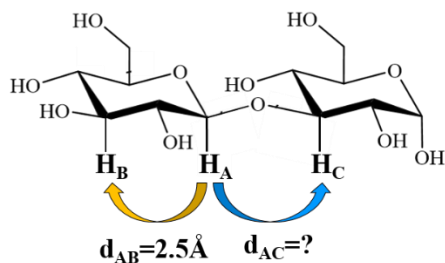
Figure 1.3.3 (Above) Other display of equation 1.7, where I are the experimental intensities of the NOEs signal between A-B and A-C, d_{AB} is the know distance between A and B; (Below) Representation of the torsion angles in αGlc1-6αGlc disaccharide with an example of the possible NOEs.

1.3.2.3 Saturation Transfer Difference

STD is a robust and powerful experiment for identifying ligand-receptor interactions, employing usually ^{1}H-NMR experiments.

It is based on the strikingly different relaxation properties that take place for small molecules and their large receptors. In large biomolecules, the cross-relaxation mechanisms that provide NOEs are very efficient due to the small motion (long correlation times) and to the large network of protons that are coupled through space. Thus, an irradiation pulse applied on a given frequency range will saturate a specific group of protein protons. By extensive cross relaxation (a phenomenon called spin diffusion), the initial saturation is easily transferred to the vicinal protons and transmitted throughout the whole receptor. If the protein binds to the ligand, this saturation is also transferred to the ligand protons through dipolar coupling. For this reason, the signals of the ligand protons in close contact with the protein (distance < 5Å) decrease and the degree of this saturation depends on the proximity of the ligand nuclei at the protein (Fig. 1.3.4). Therefore, besides suggesting the presence of an interaction, the

observed changes in the intensity of the ligand signals can also be used to define the region that is in intimate contact with the protein (ligand epitope). [53,54]
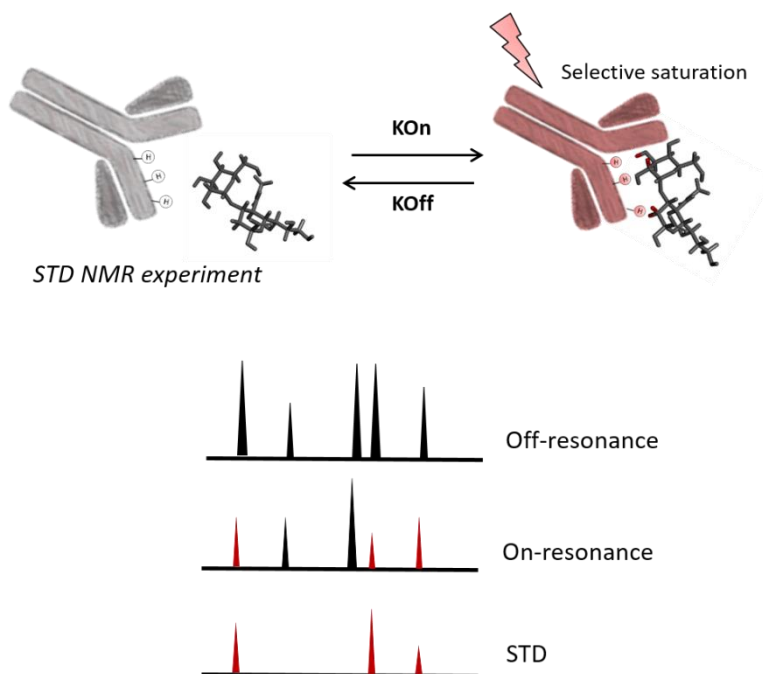
Figure 1.3.4 *General scheme of a STD experiment. Closer nuclei of the ligand receive higher saturation from the receptor while nuclei far from the receptor are not affected.*

The STD NMR experiment is based on difference spectroscopy: To visualize the intensity changes in a simple manner, a second spectrum "off resonance", is also recorded. In this case, the irradiation takes place in a spectral region where neither the signals from the ligand and protein are present. The STD spectrum results in the subtraction of the two spectra (Off-resonance – On-resonance) and all ligand signals not in close contact with the protein are cancelled out. Only those directly in contact with the protein have felt the saturation, display different intensities in on and off-resonance experiments and, therefore, appear in the STD NMR spectrum. (Fig. 1.3.4). [55]

The degree of ligand saturation depends on the residence time of the ligand in the protein-binding pocket. Saturation of the protein and the bound ligand is very fast (about 100-200 ms). Therefore, a fast off-rate of the ligand transfers the information about saturation rapidly into solution. The best STD signals are observed for systems with moderate affinity constants ($K_d \approx 10^{-8}$-10^{-3} M). In fact, if binding is very strong or too weak, the result is a weak or absent STD signal. [56]

The experiment is performed using large ligand/receptor molar ratios. Therefore, the proportion of saturated ligands in solution increases during the saturation time, and the information on the bound state resulting from the saturated protein is amplified, which means that only a relatively small amount of protein is required (ca. 10-20μM) with typical 1:20 to 1:100 receptor-ligand molar ratios.

1.3.3 Computational Chemistry and Saccharides

1.3.3.1 Molecular dynamics (MD) simulations

Given the intrinsic flexibility of oligo and polysaccharides, the detailed conformational analysis obtained from NMR is usually assisted by computational methods, especially MD simulations.

MD simulations provide information on the major three-dimensional structure and dynamics in particular time scales of a given molecule in solution. Indeed, for polysaccharides, NMR techniques may define define ''local'' conformational features of a given molecule (the glycosidic linkage and ring geometries), but to a ''general'' view of the shape of the polymer, as compactness/extension of the molecule, is impossible to define through NMR alone. In contrast, MD may predict the presence of different conformers in solution and their relative populations, providing geometrical features that can be correlated with the experimental NMR data. Thus, expected average distances and torsion angles between nuclei can be extracted, which can be used to estimate NMR parameters, as NOEs and coupling constants. These estimates can be compared to the NMR

experimental data to propose a 3D model or a conformational ensemble that accounts for the observations. For these reasons, computational chemistry methods, and in particular MD, are important tools for defining structural features of biomolecules.[57]

MD simulations provide a full description of the system's evolution as function of time, what is called trajectory.[58,59,60,61] These trajectories are calculated by solving the equations of motion of Newton (Eq. 1.8). The forces between atoms and their potential energies are calculated using a particular molecular force field, which should be suitable for the particular type of molecule under evaluation. The choice of a particular force field over another can greatly influence the result obtained. For this reason, the selection of the correct force field is very important. Saccharides, with their anomeric effects and flexibility issues, are very particular molecules, as described above.

$$\frac{d^2 x_i}{dt^2} = \frac{F x_i}{m_i}$$

Equation 1.8 *$F x_i$ is the force acting on particle i of mass m_i at position x_i and time t.*

A standard method for solving the Equation 1.8 is called the *finite difference approach*. The coordinates and velocities of a molecule at a time *$t + \Delta t$* are obtained from the molecular coordinates and velocities at a previous time *t*. The repetition are reproduced until sufficient time steps have been collected. The choice of a time interval *Δt* is important for avoiding unrealistic oscillations of the system. In particular, the time step should be less than the fastest moving period simulated by the system under test.

From the knowledge of the force on each atom in the system, it is then possible to determine their accelerations. Integration of the equations of the motion then yields a trajectory that describes the positions, velocities and acceleration of the particles as they vary with time. From this trajectory, the average values of properties can be determined.

The software that has been used herein is the AMBER package,[62] with the specific force fields optimized for carbohydrates called GLYCAM (the GLYCAM06j-1 version[63]). For the mimetics, the GAFF (General Amber Force Field) has been employed, which is optimized for small organic molecules.[64]

MD simulations are typically carried out in four steps. In the first one, the system is built and submitted to several minimization cycles. In particular, a first phase of fast minimization (steepest descend), and a second one, more refined, where the coordinates of the atoms are gradually changed in the search of a minimum of energy (conjugate gradient). The second step consists on heating the system to remove the bad contacts and on a gradual scaling of the velocities. The third step is called equilibration step, and consists on a short MD simulation (2ns) that ensure the stability of the system. The last step is the production phase in which the actual MD simulation is performed. Herein, the trajectory is generated and stored for further analysis.

The major purpose of these MD simulations is to predict and reproduce the behavior of biological systems that exist, in nature. Thus, usually, a solvated environment is employed. The most reliable way to model an aqueous medium is to create a solvent box around the molecule, with discrete solvent molecules explicitly included in the simulations. There are different water models, which differ in the complexity of the employed parameterization and they may display different behaviors during the MD simulation.[65] The simplest and the most commonly used model is the TIP3P.[66] This model is characterized by three interaction sites, corresponding to the three atoms of the water molecule arranged to form an angle of 104,5°. The assigned charges are O = -0.834 and H = +0.417.

The MD simulations have become much more accessible and powerful in the last few years. The recently introduced computer hardware, particularly the graphics processing units (GPUs), allows powerful simulations to be run locally at a modest cost. This fact has given the opportunity to greatly expand the complexity of the molecules studied,[67] with simulation times beyond microseconds.[68,69]

1.3.3.2 Quantum Mechanics (QM) calculations

When the molecular structure is critically determined by electron delocalization, it is not possible to neglect the energy contribution coming from the stabilizing molecular orbital interactions. This is the case for saccharides, where the conformation around the glycosidic linkage is largely driven by the anomeric effects. For these systems, the structural problem has to be solved considering the electrons as discrete particles or as a cloud, not restricted to the proper nucleus. Highly expensive computational methods are then necessary. However, if the molecule is not too large, QM calculations can be achieved in a reasonably time and the resulting data are usually very accurate. All QM methods ultimately trace back to the Schrödinger equation (Eq. 1.9).

$$H\Psi=E\Psi$$

*Equation 1.9 Where **H** is the energy operator that describes the kinetic and potential energy of an electron in a field of nuclei and other electrons. Usually, the nuclei are assumed to be stationary. **Ψ** is f(x,y,z), a set of spatial distributions describing the probability of finding electrons (orbitals), and **E** is a sum of the energies of the orbitals, which may contain 1 or at most 2 electrons.*

For a molecular system, which obviously includes more than one electron, the Schrödinger equation cannot be solved, and thus approximations need to be introduced to provide practical results. The different kinds of approximations and their choice depend on the molecular system under study.[70,71]

The software used herein has been GAUSSIAN 09, a general purpose computational chemistry software package initially released in 1970 by Nobel laureate John Pople.[72] Gaussian is capable of predicting many properties of molecules and reactions, including molecular energies and structures, energies and structures of transition sates bond and reaction energies, molecular orbitals, atomic charges and electrostatic potential, vibrational frequencies and NMR properties (J couplings and chemical shift). The computations can be carried out on systems in the gas phase or in solutions (implicit solvent).

Gaussian approximates orbital shapes and orbital energies of a given molecular geometry using a model chemistry consisting of two parts: a basis set and a method. The combination of a method and a basis set represents the level of theory that will be used during the calculations.

There are several methods that differ mainly according to how the tendency of electrons to avoid each other is treated, even within the same orbital (electron correlation). The most common are four:

1) The Semi-empirical method uses pre-calculated orbital functions for different kinds of atoms. It is the fastest. However, it has a low computational cost and, for the same reasons, it is the least accurate.
2) The Hartree-Fock (HF) method ignores the electron correlation and uses the many-electron wavefunction (Ψ) that is estimated by the self-consistent field (SCF) method.
3) The Density Functional Theory (DFT) considers the electron correlation by estimating the interaction of an electron with the total electron density (*1.2.3.3*).
4) The Møller-Plesset *n* (MP2, MP3) methods are *post*-Hartree-Fock methods that take into account the electron correlation by estimating the interaction of the electron pairs.

HF, DFT and MP*n* are *ab initio* methods that require significant computing power to ensure the generation of accurate results. The employed basis sets are linear combinations of basis function that approximate the molecular orbitals (MOs). There are different ones and the choice depends on the particular problem under evaluation.

1.3.3.3.1 Density Functional Models

The density functional theory (DFT) assumes that the sum of the exchange and correlation energies of a uniform electron gas can be calculated knowing only its density. The main advantage in DFT is that, unlike the wave function, the electron density is an observable and can be measured experimentally, e. g. by

X-ray diffraction. This approximation assumes that it is possible to reduce the number of electrons that are in the molecule to a single electron density, thus considerably reducing the computational cost. The physics-mathematics description of the equations behind DFT is beyond the scope of this thesis, and just a brief discussion of the main properties of the electron density is presented.

i) The density integrates to the number of electrons; this means that the density is a function of all the electrons in the molecule.

ii) The density has maxima only at the nuclei positions. In others words, the density takes into account the attractive forces exerted by the positive charge of the nuclei.

iii) The density at the position of the nucleus contains information on the nuclear charge Z, thus definingthe chemical nature of the molecular constituent elements.

iv) The theory includes a term for the exchange and correlation electron interaction. This means that solutions are given to the Coulombic repulsion and exclusion Pauli principle problems.

Thus, the electron density already provides all the required ingredients for a complete characterization of the electronic structure in a given molecule. The success of DFT in the computational chemistry field has been largely demonstrated. For saccharides, numerous applications have dealt with the structural characterization of mono- and oligo-saccharides, given the importance of the anomeric effects to define the molecular geometry and energy of this family of molecules.[73,74,75,76,77,78]

General objectives

The primordial scientific aim of this Thesis project is the characterization of the conformation, dynamics and interaction features of different capasular polysaccharides related to infectious diseases. In particular, and within the frame of the GlycoVAX project, we have focused on the *Neisseria meningitidis (Men) and* Group B *Streptococcus (GBS).*

One major aim, for the Men family, has been unraveling the fine details of the factors that modulate the conformational, dynamics, and presentation features of the Men A, X, C, W and Y natural polysaccharides, along with different fragments and glycomimetics thereof. In the case, of GBS, the targets have been the GBS Ia, Ib, II, III, IV and V polysaccharides.

One additional goal has been to deduce the binding features of some of these polysaccharides to their corresponding monoclonal antibodies.

These scientific objectives have been intimately related to the training aims, focused on the acquisition of high-level knowledge in chemical biology, with emphasis in conformational analysis and molecular recognition, especially focused in state-of-the-art NMR methods and their applications to problems of biological interest, as well as in their combination with computational tools.

Chapter 2

Neisseria meningitidis

The work presented in this chapter has been performed in collaboration with:

- GSK Glycoconjugate research team in Siena (Dr. Roberto Adamo) that has provided the different molecules that have been studied by NMR and the specific mAbs used in the interaction studies.

Publications:

(1) ''The Conformation of the Mannopyranosyl Phosphate Repeating Unit of the Capsular Polysaccharide of Neisseria meningitidis Serogroup A and Its Carba-Mimetic'' **Ilaria Calloni**, Luca Unione, Gonzalo Jiménez-Osés, Francisco Corzana, Linda Del Bino, Alessio Corrado, Olimpia Pitirollo, Cinzia Colombo, Luigi Lay, Roberto Adamo and Jesús Jiménez-Barbero. *Eur. J. Org. Chem*. **2018**, 4548–455.

2.1 Introduction

Neisseria meningitidis is a Gram-negative bacteria, member of the nasopharyngeal microbiome in healthy people, which can cause septicemia and meningitis in susceptible individuals. Since it is a strict human pathogen and most patients have not been in contact with other cases, is acquired person-to-person contact via nasal or oral secretions. [79,80] Meningococcal meningitidis, caused by this bacteria, is associated with high deadliness (over 50% when untreated) and high rate of consequences for the survivors, including amputation, brain and neurologic damage.[81,82] The disease is observed in a range of different situations: from sporadic cases to huge pandemics. It can affect any age although it mainly involves infants or adolescents/young adults [83]. The geographic distribution is different for the different serogroups. (Fig 2.1.1) The most problematic region is sub-Saharan Africa, extending from Senegal in the west to Ethiopia in the east, with 30000 cases reported each year.[84,85]

The treatment of this disease includes the use of appropriate antibiotics, as penicillin, ampicillin and ceftriaxone, which must be started as soon as possible from the onset of the disease. Unfortunately, the occurrence of antibiotic resistance and lack of complete effectiveness of the available treatments makes this disease a substantial and evolving therapeutic challenge.[86] For these reasons, mass preventive immunization campaigns using specific vaccines against meningococcal disease are essential.[87]
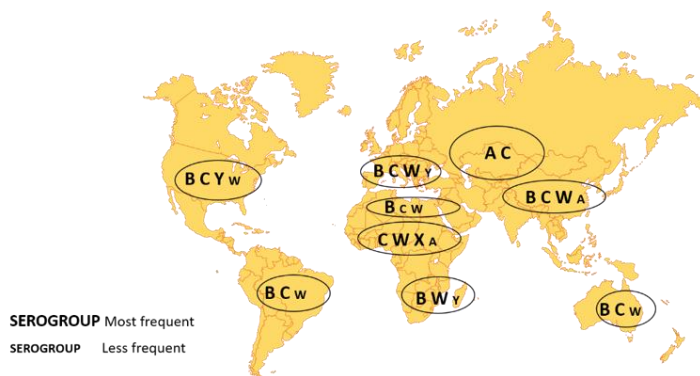
Figure 2.1.1 *Map of the predominant Neisseria meningitidis serogroups by geographic location in 2018. Data obtained from World Health Organization.*

There are thirteen different serogroups, which differ in the chemical composition of their capsular polysaccharides (Table 2.1.1) that recovered the bacterial cell surface and behave as the primary virulence factors. Six of them (A, B, C, W, Y and X) are very dangerous and can cause epidemics.[88]

The capsular polysaccharides of serogroup B and C are composed of polysialic acid, or sialic acid (neuraminic acid, Neu5Ac) linked to glucose (Glc) in the serogroup Y or galactose (Gal) in W.[89] The capsules of group A and X have a more peculiar structure and are composed of N-acetylmannosamine (ManNAc, A) and N-acetylglucosamine (GlcNAc, X), with the presence of a phosphate group at the glycosidic linkage.[90,91]

Type A	→6)-α-D-ManpNAc(3/4OAc)-(1→OPO$_3$→
Type X	→4)-α-D-GlcpNAc-(1→OPO$_3$→
Type B	→8)-α-D-NeupNAc-(2→
Type C	→9)-α-D-NeupNAc(7/8OAc)-(2→
Type W	→6)-α-D-Galp-(1→4)-α-D-NeupNAc(7/9OAc)-(2→
Type Y	→6)-α-D-Glcp-(1→4)-α-D-NeupNAc(7/9OAc)-(2→

***Table 2.1.1** Idealized structures of the repeating units of the six meningococcal polysaccharides responsible of epidemics.*

2.1.1 Vaccination - state of the art

Vaccines against meningococcal infections have been available for more than 40 years, although no universal vaccine is not yet available. The vaccines on the market are serogroup's specific and provide different degrees of duration of protection. Globally, we can distinguish three types of vaccines, polysaccharide vaccines, conjugate vaccines, and protein-based vaccines.

The first ones have been used as answers to outbreaks, mainly in Africa. They can be bivalent (serogroups A and C), trivalent (serogroups A, C and W), and

tetravalent (serogroups A, C, Y and W). However, these type of vaccines display the typical polysaccharide vaccines problems: they are not effective before two years of age, they only offer three years of protection and do not produce herd immunity.[87,92,] The conjugate vaccines have been typically used for prevention, although they have also been employed for outbreak responses. They provide long-lasting immunity (5 years), induce herd immunity and can be used from one year of the age. There are different available glycoconjugate vaccines, as the MenAfriVac, a serogroup A conjugate. Between 2010 and 2017, over 270 million doses of these vaccine have been distributed, achieving a drastic reduction of this meningococcal disease.[93,94] However, the reduction in the incidence of serogroup A has caused the increase of occurrence of the other serogroups. Cases caused by serogroups C, W and X have been reported in Burkina Faso, Niger and Nigeria. Thus, there is a real need to develop new multivalent vaccines. A pentavalent ACWXY conjugate vaccine (NmCV-5, Serum Institute of India)[95] has successfully entered in a pivotal phase-3 clinical study (ClinicalTrials.gov Identifier: NCT03964012). Moreover, three tetravalent meningococcal conjugate vaccines are available (MenACWY), containing polysaccharides from serogroups A, C, W and Y conjugated to different carrier proteins: tetanus toxoid (Nimenrix; Pfizer), diphtheria toxoid (Menactra; Sanofi-Pasteur), or CRM197 (Menveo; GlaxoSmithKline).[96,97]

2.2 Goals

Since structure and function are intrinsically correlated, herein we aimed at deducing the three-dimensional structures and dynamic features of the Men A, X, C, W and Y natural polysaccharides. Specifically, for Men A, the conformation of the natural molecules and some mimetics thereof. For Men C, Men W and Men Y, the role of acetylation in the conformation and presentation of the molecule. Moreover, we also aimed at exploring the molecular recognition features of the interactions of Men C and W with their specific mAbs.

For that, it was required to establish a robust methodology, based on the synergic application of a series of NMR experiments (TOCSY, NOESY, HSQC and STD) assisted by molecular modelling methods, in particular molecular dynamics simulations and, when possible, *ab initio* techniques.

2.3 Results and discussion

2.3.1 *Neisseria meningitidis* serogroup A and comparison with its mimetics

Neisseria meningitidis serogroup A (MenA) capsular polysaccharide consists of (1→6)-linked ManNAc-1-phosphate repeating units (Figure 2.3.1), predominantly O-acetylated at 3-OH (80%). This polysaccharide suffers from chemical liability in water, and therefore it is only preserved at low temperatures or lyophilized formulations. The reason for this instability seems to be the presence of a phosphodiester linkage at the anomeric position together with the axially-oriented *N*-acetyl group at position 2 of the mannosamine moiety, which can assist the departure of the phosphomonoester group by facilitating the cleavage of the C1–O1 bond. [98]

Thus, the design and synthesis of novel and hydrolytically stable structural analogues of MenA CPS is of paramount importance. The hydrolysis of the glycosidic linkage can be prevented by chemical modification of the glycosyl 1-O-phosphates moiety using sugar mimicry, where a methylene group replaces either the endo-cyclic oxygen atom at the pyranose ring[99] (Figure 2.3.1) or the interglycosidic oxygen[100,101] (Figure 2.3.1). The aim of this study is to determine which analogue could better mimic the natural structural features and to achieve the stimulation of immune response in host-pathogen interactions.

Using computational chemistry and molecular modelling methods, in particular, ab-initio techniques and molecular dynamics simulations, we have deduced the lowest energy structure (global minimum), as well as other possible secondary geometries.

Fig. 1: Repeating unit of Men A CPS
R= H or Ac (80%)
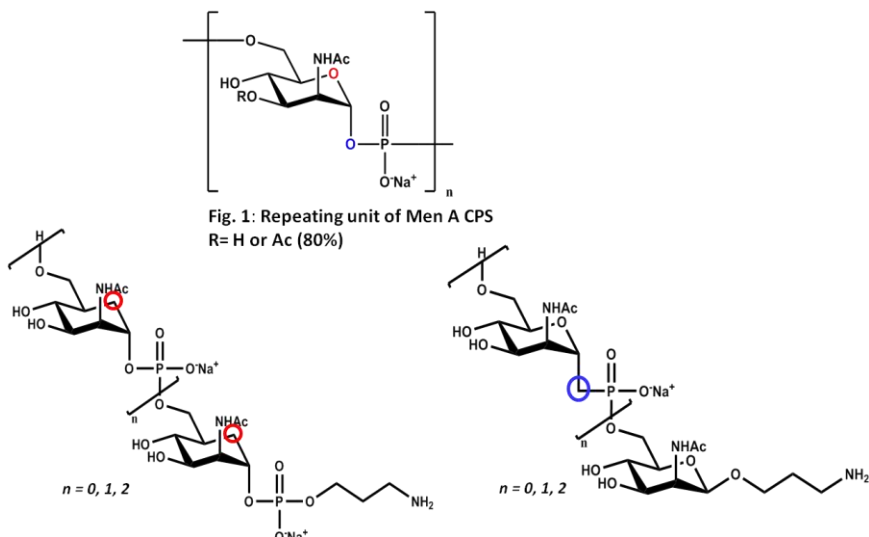
Figure 2.3.1 The natural monomer of Neisseria meningitidis A capsular polysaccharide and its carba and C-glycosyl-mimetics.

Computational analysis on derivatives **1a** and **1b** (with a methyl phosphodiester linked at the anomeric and primary hydroxyl, respectively) and their C-carba glycomimetics **2a** and **2b** (Figure 2.3.2) were performed. The results were validated by NMR experiments, performed on synthetized monosaccharides **1c** and **1d** and their corresponding carba-analogues **2c** and **2d** (Figure 2.3.2).
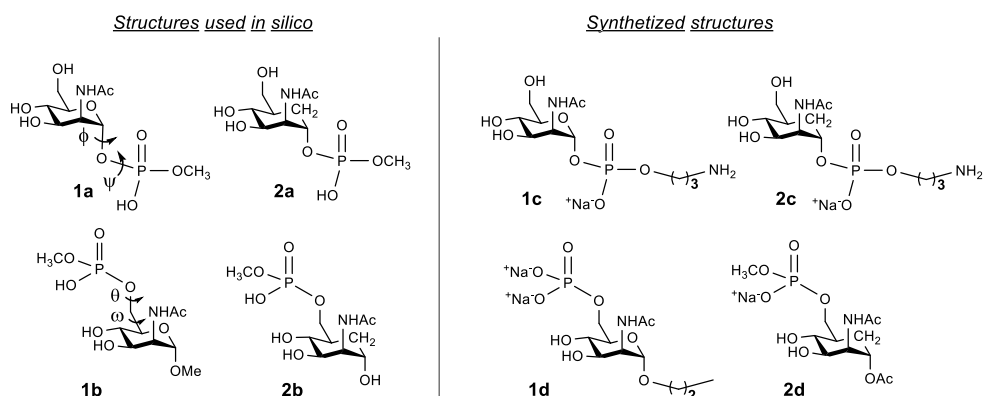
*Figure 2.3.2 Schematic view of the structures of the studied compounds. Model compounds **1a** and **1b** and their C-carba glycomimetics **2a** and **2b** were subjected to in silico studies. Synthetic compounds **1c** and **1d** and their corresponding carba-analogues **2c** and **2d** were used for NMR studies.*

2.3.1.1 The conformation of 1a, 1c and 2a, 2c

For compound **1a**, a long (1.5 µs) MD simulation (Figure 2.3.3a) was performed using the GLYCAM06 force field, specific for carbohydrate molecules, using explicit solvent molecules (water) and periodic boundary conditions. The results indicate that there is a very major preferred conformation in terms of ϕ/ψ. As expected for a natural sugar **1a**, the ϕ value is consistent with the *exo-syn* conformation (Figure 2.3.4). Indeed, the stereoelectronic contribution of the exo-anomeric effect strongly stabilizes this geometry. For ψ, the -60 value is largely populated. Obviously, there is certain motion around the corresponding global minimum, with minor excursions to other regions of the conformation map.

A similar analysis was performed with **2a**. However, in this case, the MD simulation of the carbasugar mimic, (Figure 2.3.3b) performed with the GAFF11 force field, suggested that the molecule displays a conformational equilibrium, with a major contribution of the *non-exo* form, which is not present in the natural compound. There is is also a larger flexibility around ψ torsion with major variability on the corresponding angle values.
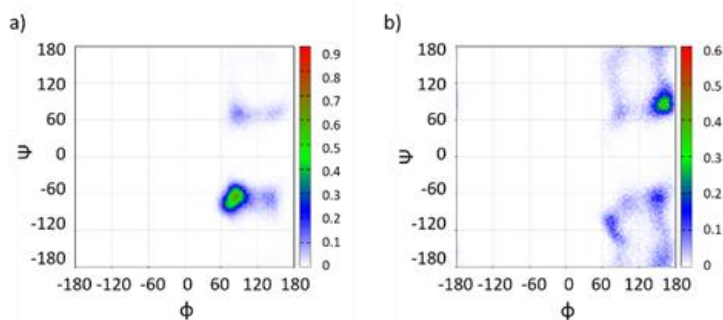
Figure 2.3.3 *(a) ϕ/ψ plot of the 1.5 µs MD trajectory of in explicit water (GLYCAM06 force field) for **1a**; (b) ϕ/ψ plot of the trajectory of 1 µs of MD simulations in explicit water (GAFF11 force field) for **2a**.*

The energy profile for **1a** around ϕ for the best ψ value was then evaluated using *ab initio* calculations with Gaussian09 (DFT calculations with B3LYP combined with the 6-31++g(d,p) basis set) to estimate the energy difference between the different possible local minima. The calculated minima for the three possible

staggered rotamers are given in Table 2.3.1. Again, the *exo-syn* conformer is highly stabilized versus the alternative non-exoanomeric orientation for a natural sugar **1a**, while for a carbasugar mimic **2a** the contribution of the *non-exo* form is greater. The *exo-anti* geometry, which is highly destabilized due to steric hindrance (Figure 2.3.4), presents a high level of energy for both molecules. On the other hand, the quantum mechanics QM calculations for **2a** showed that the *exo-syn* and *non-exo* conformations display very similar energy values (Table 2.3.1).

	ΔE (kcal/mol)	
	1a	**2a**
exo-syn	0	1.5
non-exo	2.3	0
exo-anti	7.1	5.8

Table 2.3.1 *Calculated energy difference between the three staggered conformations around ϕ: exo-syn, non-exo and exo-anti conformations for the natural compound **1a** and its carba-glycomimetic **2a**. The single-point energy was calculated using Gaussian09 (B3LYP combined with 6-31++g(d,p) basis set).*

	$^3J_{\text{H1,P}}$	$^3J_{\text{P,C2}}$	$^2J_{\text{P,C1}}$
Exp (**1c**)	7.7	8.9	5.5
DFT calculation for *exo-syn* (**1a**)	6.6	9.0	6.9
DFT calculation for *non-exo* (**1a**)	0.9	0.4	3.3
DFT calculation for *exo-anti* (**1a**)	19	4.2	12.3

Table 2.3.2 *Comparison between the theoretical (**1a**) and experimental (**1c**) J couplings (Hz) for the three staggered orientations around ϕ. The theoretical values were calculated with B3LYP/6-31++g(d,p) basis set and the GIAO method. The agreement between the expected values for the exo-syn conformer and the experimental values is remarkable.*
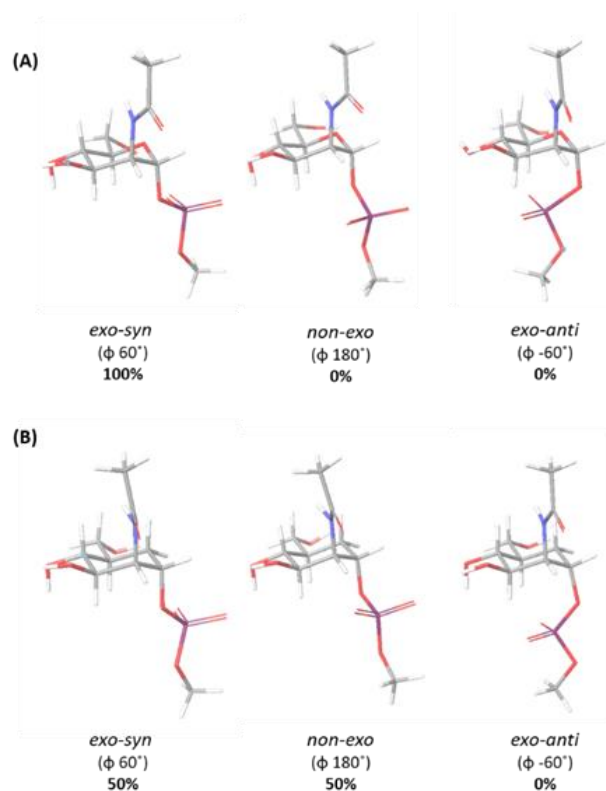
Figure 2.3.4 Representation of the exo-syn, non-exo, exo-anti conformers for: compound *1a* (A) and compound *2a* (B).

These theoretical results were compared to those obtained through experimental NMR methods with compound **1c**. Different NMR experiments (^{1}H, ^{1}H {^{31}P}, ^{1}H-^{31}P COSY, ^{13}C {^{1}H}, HSQC) were performed to obtain the key NMR parameters with conformational information that could be compared to the theoretical predictions. In particular, special attention was paid to obtain the *J* couplings that define the conformation around ϕ and ψ torsion angles (Figure 2.3.2). In particular the $^3J_{H1,P}$, $^3J_{P,C2}$, and $^2J_{P,C1}$ values were determined (Table 2.3.2). Regarding ϕ, the comparison between these experimental values with those estimated from *ab initio* calculation for the three major conformations of **1a** permitted to demonstrate the presence of *exo-syn* (Figure 2.3.4) as the predominant conformation for **1c** in solution. In particular, $^3J_{H1,P}$ and $^3J_{C2,P}$ showed a clear preference for this geometry. The geminal $^2J_{P,C1}$ is also consistent with a major *exo-syn* conformation.

A similar analysis was performed with the carba-analogue **2c**, to compare the theoretical predictions made on **2a** with experimental NMR methods. Again, special attention was paid to $^3J_{P,C5'}$, $^3J_{P,C2}$ and $^2J_{P,C1}$, the *J* couplings that define the conformation around ϕ and ψ dihedral angles. The comparison between these experimental values with those estimated from *ab initio* calculation for the three major conformations of **2a** (Table 2.3.3) allowed defining the population of the different conformers of **2c** in solution. Fittingly, in this case, the data supported the existence of two equal populations 50% *exo-syn* and 50% *non-exo* for the conformers around φ dihedral angle (Figure 2.3.4). The estimation fully agrees with the lack of exo-anomeric stabilization for the carba-analogue. In the absence of stereoelectronic effects, the expected steric interactions (Figure 2.3.4) are fairly similar for the two possible orientations around ϕ.

	$^3J_{PC,5'}$	$^3J_{P,C2}$	$^2J_{P,C1}$
Exp	3.1	3.8	4.8
DFT calculation for [50%]*exo-syn* [50%]*non-exo* (**2a**)	3.4	4.1	4.9
DFT calculation for *exo-syn* (**2a**)	0.5	7.5	0.6
DFT calculation for *non-exo* (**2a**)	6.3	0.8	9.2

Table 2.3.3 *Theoretical (**2a**) and experimental (**2c**) J couplings for the three major orientation of the φ dihedral angle for carba-analogues **2a/2c**. The theoretical values have been calculated with B3LYP/6-31++g(d,p) basis set and GIAO method.*

2.3.1.2 The conformation of 1b, 1d and 2b, 2d

The analysis of the long (1.5 μs) MD simulation performed for **1b** (Figure 2.3.5a) using the GLYCAM06 force field indicated that there is a major conformation in terms of ω/θ. As expected for a natural sugar, the ω value corresponds to the gauche-gauche (gg) conformation around C5-C6. For θ, the results indicated the existence of two different populations. The major conformation corresponds to a -120˚ value, while the anti geometry (180˚) is also present as a minor conformer, with certain flexibility around the corresponding minima.

The analysis of the results of the long (1µs) MD simulation for the carba-analogue **2b** (Figure 2.3.5b), performed using the GAFF11 force field, showed a conformational equilibrium mixture between the gauche-gauche (gg) and gauche-trans (gt) orientations, with a very minor participation of the trans-gauche (tg) conformer, as indicated by ω. However, for θ, the anti-geometry value is now the only populated conformation.
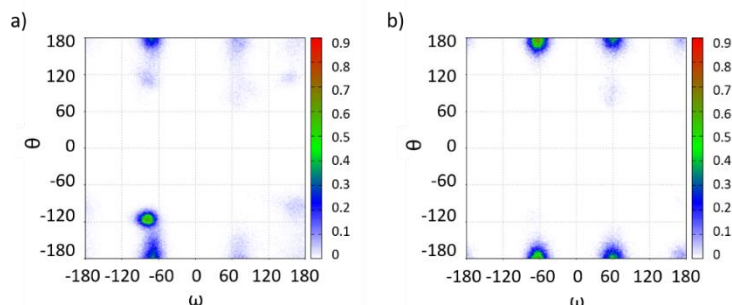
Figure 2.3.5 *(a) ω/θ plot of the trajectory of the 1.5 µs of molecular dynamics simulations in explicit water (GLYCAM06 force field) for compound **1b**; (b) ω/θ plot of the trajectory of 1 µs of molecular dynamics simulations in explicit water (GAFF11 force field) for **2b**.*

The energy profile around ω for the best θ value was evaluated using *ab initio* calculations with Gaussian09 (DFT calculations with B3LYP combined with the 6-31++g(d,p) basis set) to estimate the energy difference between the different possible local minima. The calculated minima for the three possible staggered rotamers (Figure 2.3.6) of **1b** and carba-analogue **2b** are given in Table 2.3.4.

The *ab initio* results also support that the gg conformer is highly stabilized versus the alternative gt and tg orientations.

	ΔE (kcal/mol)	
	1b	**2b**
gg	0	0
gt	6.2	4.6
tg	14.2	4.5

Table 2.3.4 *Calculated energy difference between the three major conformations around ω: gg, gt and tg conformations for compounds **1b** and **2b**. The single-point energy was calculated using the Gaussian09 (B3LYP combined with 6-31++g(d,p) basis set).*

Again, these theoretical results obtained for natural sugar **1b** and carba-analogue **2b** were compared to those obtained through experimental NMR methods with synthetic compound **1d** and carba-analogue **2d**, respectively.

For compound **1d**, in addition to the previously described NMR experiments, a *J*-resolved experiment was also performed to obtain the key NMR parameters with conformational information. In particular, $^3J_{H5,H6a}$ and $^3J_{H5,H6b}$ values define ω orientation, while $^3J_{H6a,P}$, $^2J_{H6b,P}$, and $^3J_{C5,P}$ are related to θ torsion angle. The comparison between these experimental values with those estimated from *ab initio* calculation for the three major conformation of **1b** (Tables 2.3.5-2.3.6) permitted to assess the exclusive presence of the gg rotamer as the predominant conformation in solution for **1d**. Regarding θ, the experimental data permitted to define that its major conformation corresponds to the anti geometry (θ= 180˚), while the eclipsed conformation (θ= 120˚) is also present in a minor amount.

	$^3J_{H5,H6a}$	$^3J_{H5,H6b}$
Exp (**1d**)	2.1	3.1
DFT calculation for gg (**1b**)	1.4	3.1
DFT calculation for gt (**1b**)	1.7	8
DFT calculation for tg (**1b**)	8.5	3.4

Table 2.3.5 *Theoretical (**1b**) and experimental (**1d**) J couplings for the three major orientations of ω angle. The theoretical values have been calculated with B3LYP/6-31++g(d,p) basis set and GIAO method.*

	$^3J_{H6a,P}$	$^2J_{H6b,P}$	$^3J_{C5,P}$
Exp (**1d**)	3	4.5	7.5
DFT calculation for [80%]anti [20%]eclipsed (**1b**)	3.6	4.2	7.6
DFT Calculation for θ 180˚(**1b**)	1.8	2.2	9
DFT Calculation for θ -120˚ (**1b**)	11	12	2

Table 2.3.6 *Theoretical (**1b**) and experimental (**1d**) J couplings for the three major orientations of the θ torsion angle for **1b**. The theoretical values have been calculated with B3LYP/6-31++g(d,p) basis set and GIAO method.*

For compound **2d**, the comparison between the experimental $^3J_{H5,H6a}$ and $^3J_{H5,H6b}$ values with those estimated from the *ab initio* calculations for **2b** (Table 2.3.7) indeed supported the theoretical predictions and suggested populations in solution ca. 60% gg and 40% gt for ω.

	$^3J_{H5,H6a}$	$^3J_{H5,H6b}$
Exp (**2d**)	2.7	5.2
DFT calculation for gg (**2b**)	2.4	2.2
DFT calculation for gt (**2b**)	3.8	9.6
DFT calculation for tg (**2b**)	9.5	4
DFT calculation for [60%]gg [40%]gt (**2b**)	2.9	5.1

Table 2.3.7 *Theoretical (**2b**) and experimental (**2d**)J couplings for the three major orientation of the ω dihedral angle. The theoretical values have been calculated with B3LYP/6-31++g(d,p) basis set and GIAO method.*

2.3.1.3 Comparison of the conformation of the oligosaccharides

The conformational and dynamic behaviour of the natural (Fig 2.3.6a) MenA capsular polysaccharide (CPS) and its carbasugar analogue (Fig 2.3.6b) has also been analysed by using MD simulations. Trimer fragments of both molecules were built and submitted to the MD analysis.
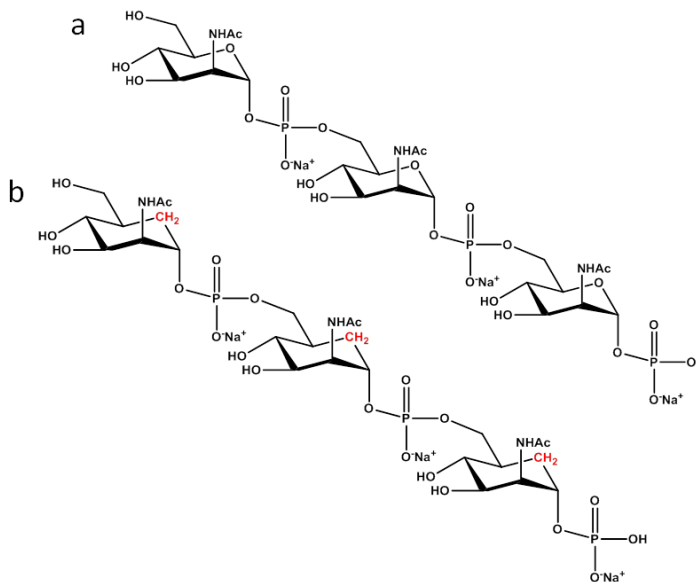
Figure 2.3.6 *(a) The natural Neisseria meningitidis A capsular polysaccharide, showing three repeats; (b) Structure of the carbasugar mimetic employed herein, previously described in Org Biomol Chem **2009**, 7, 3734 and Org Biomol Chem **2012**, 10, 6673.*

The torsion angles are defined as follows:

ϕ = O5-C1-O-P, Ψ = C1-O1-P-O, ω=O6-C5-C6-O and θ=C5-C6-O-P, for the natural compound ϕ = C5a-C1-O-P, ψ = C1-O1-P-O, ω=C5a-C5-C6-O and θ=C5-C6-O-P, for the carbasugar.
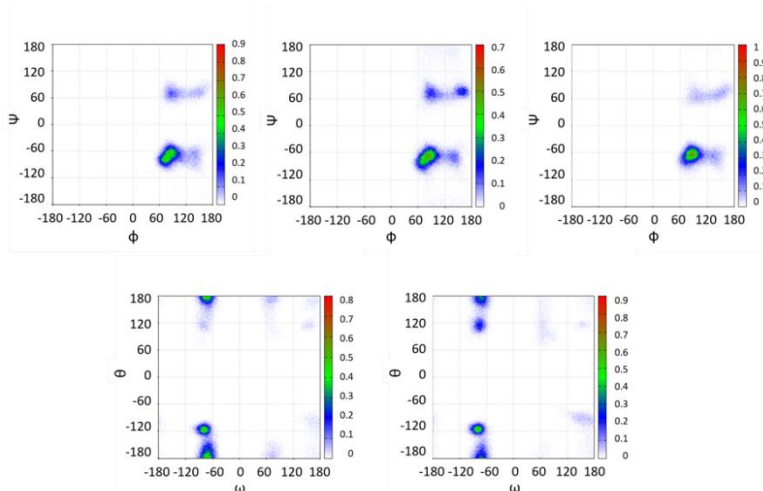
Figure 2.3.7 *ϕ/ψ (top) and ω/θ (bottom) plots for every glycosidic linkage of the natural CPS trisaccharide, as deduced from the 500 ns MD trajectory in explicit water (GLYCAM06 force field).*

The deduced conformation around ϕ for every glycosidic linkage is predominantly exo-syn while that around ω torsions was always gg. Nevertheless, there are slight variations around the ψ and θ dihedral angles, which are generally more flexible (Fig 2.3.7).
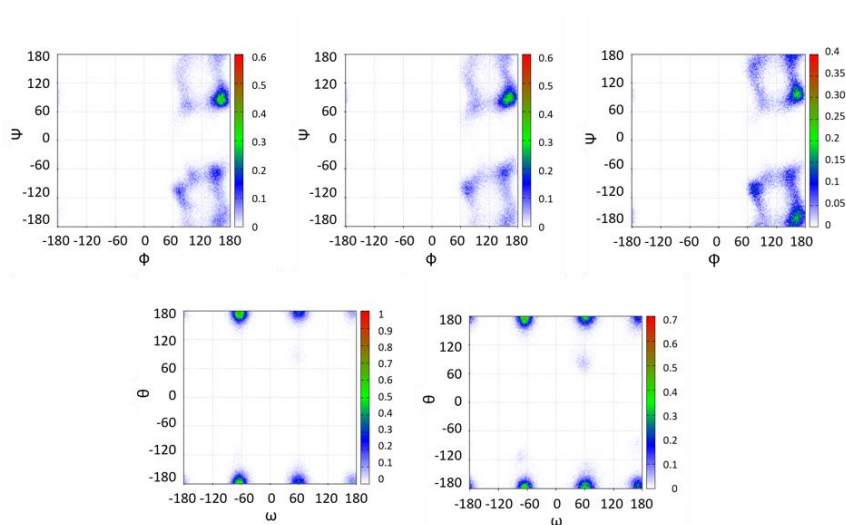
Figure 2.3.8 *φ/Ψ and ω/θ plots for every glycosidic linkage of the mimetic CPS trisaccharide, as deduced from the 500 ns MD trajectory in explicit water (GAFF12 force field).*

In contrast, there are conformational equilibria around both ϕ and ω torsions of the carba sugar analogue. In particular, a mixture of the *exo-syn* and *non-exo* geometries was deduced around ϕ, while both gg and gt contribute to the equilibrium around ω. The behaviour is very similar around every glycosidic linkage of the trisaccharide (Fig 2.3.8).

For the natural monosaccharide, the extension of the major *exo*-anomeric geometry leads to the trisaccharide structure shown in Figure 2.3.9. In this conformation, amphipathic presentation of alternative polar and lipophilic moieties would confer to the trimer a structure compatible with a helical arrangement with a pitch of six residues (Figure 2.3.10). In particular, both the

polar phosphate groups and the nonpolar methyl moieties of the acetamide substituents, responsible of this amphiphilic character, are exposed to the solvent. Therefore, this alternate presentation of polar and nonpolar patches in the trisaccharide epitope may allow it to interact with the proper receptor architecture.
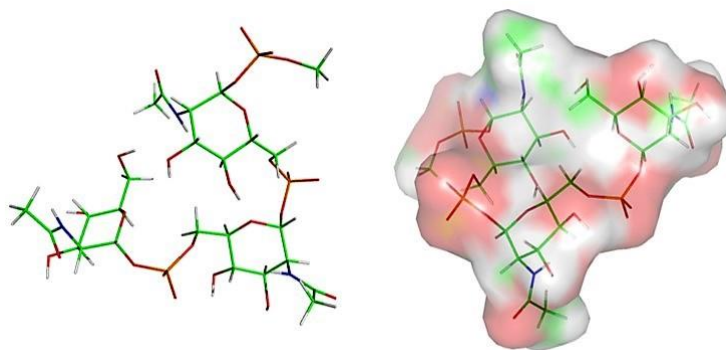
Figure 2.3.9. *Different perspectives of the major conformation predicted for a natural trisaccharide, built by extension of the major exo-anomeric conformers found for the natural monomers. On the right hand-side, a surface representation is provided, indicating the presentation of the polar phosphate groups (in color orange) and non-polar (in color green and white) methyl moieties.*
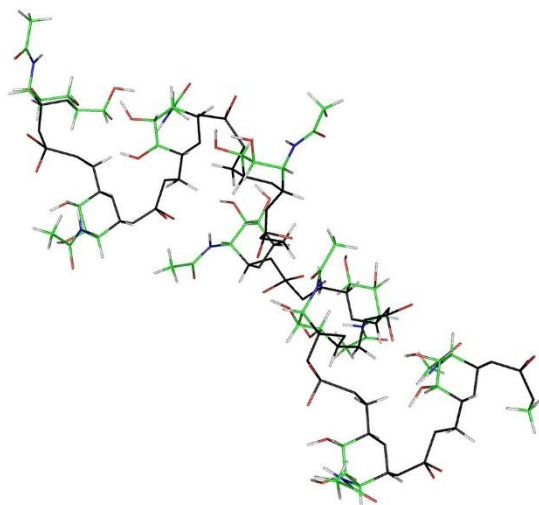
Figure 2.3.10. *Schematic representation of a putative nonasaccharide, built by extension of the exo-anomeric conformer. The amphiphilic molecule adopts a helix-like structure, with a similar orientation every 6 residues. That is, the pyranose rings of 7, 8, and 9 adopt the same presentation as 1, 2, and 3. A similar structure could also be adopted by the mimetic compound, although in much less population.*

The non-natural carba-analogue may also present a similar geometry (Figure 2.3.11), although given the presence of non-*exo*-anomeric conformers, more extended structures might also be present. Obviously, given the higher flexibility of the non-natural oligosaccharide, the selection of the required conformer for receptor binding would impose a certain entropy penalty in the putative recognition process. However, given the small energy barriers among conformers, the unfavorable energy consequences for the use of the mimetic molecule would probably be largely overcome by the improved stability of the molecule provided by the carba motif.
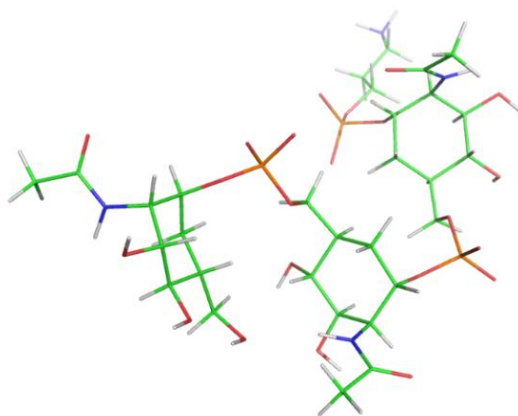
Figure 2.3.11. View of the major conformation predicted for a mimetic trisaccharide, built by extension of the exo-anomeric conformer. This geometry resembles that predicted for the natural molecule.

These computational predictions will be assessed by the experimental NMR data when the molecules become available. NMR experiments will be performed to define the geometry around the torsion angles. In particular, ^{31}P, ^{31}P {^{1}H}, ^{13}C {^{1}H}, HSQC, and *J*-resolved experiments will be employed and analysed to define the ^{2}J and ^{3}J couplings, which will permit the structure to be defined.

2.3.1.4 The conformation of the C-glycoside mimetic

A similar methodology was adopted to calculate the behaviour of the C-glycosyl analogue (Fig 2.3.1). Again, in this case, the two alternative conformations are

predicted by the *ab initio* and molecular dynamics simulations. The MD plot shows a major *non-exo* conformation around ϕ (Fig 2.3.12b), with a minor contribution of the *exo*-conformer, while the DFT results predict a similar population for both conformers. Moreover, different conformations around ω are also predicted. Obviously, these expectations should be proven by NMR experiments when the compounds became available.
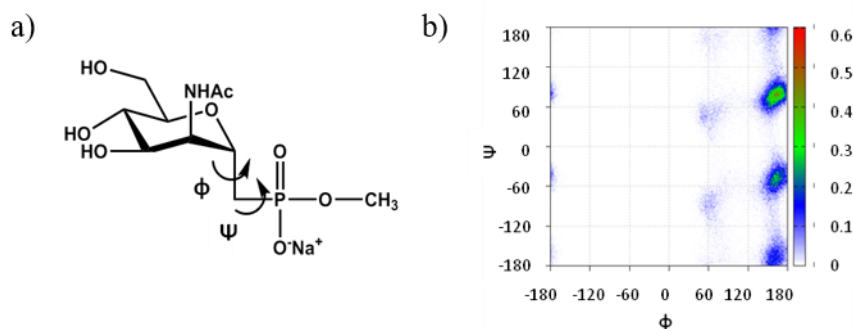
Figure 2.3.12 *(a) Representation of the structure of the C-glycosyl analogue with the definition of the key torsion angles; b) ϕ/ψ plot of the trajectory of 500 ns of molecular dynamics simulations in explicit water (GAFF force fields).*

ϕ	Δ Energy
exo-syn	0 Kcal/mol
non-exo	0.086 Kcal/mol
exo-anti	5.85 Kcal/mol

Table 2.3.8 *Calculated energy difference between the three major conformations around φ: for the C-glycosyl analogue: exo-syn, non-exo and exo-anti conformations. The single-point energy was calculated using the Gaussian09 program (DFT calculations with the 6-31++g(d,p) basis set).*

Capítulo 2.3.2 a 2.4 (ambos inclusive)sujetos a confidencialidad por la autora

Chapter 3

Group B Streptococcus

The work presented in this chapter has been performed in collaboration with:

- GSK Glycoconjugate research team in Siena (Dr. Roberto Adamo) that has provided the different molecules that have been studied by NMR and the specific mAbs used in the interaction studies.

Publications:

(**1**) ''Structural-guided design of a Group B Streptococcus type III synthetic glycan-conjugate vaccine'' Davide Oldrini, Linda del Bino, Ana Arda, Filippo Carboni, Pedro R. M. Henriques, Francesca Angiolini, Jon I. Quintana, **Ilaria Calloni**, Maria R. Romano, Francesco Berti, Jesus Jimenez-Barbero, Immaculada Margarit, Roberto Adamo. *Chem. Eur. J.* **2020**.

(**2**) ''Regioselective glycosylation strategies for the synthesis of Group Ia and Ib Streptococcus related glycans enable elucidating unique conformations of the capsular polysaccharides'' Linda Del Bino, **Ilaria Calloni**, Davide Oldrini, Maria Michelina Raso, Rossella Cuffaro, Ana Ardá, Jeroen D. C. Codée, Jesús Jiménez-Barbero, and Roberto Adamo. *Chem. Eur. J.* **2019**, 25:16277 – 16287.

3.1 Introduction

Group B *Streptococcus (Streptococcus agalactiae)* is a gram-positive bacteria that colonizes the gastrointestinal and genitourinary tracts of up to 50% of healthy adults. [120,121]

By the 1970s GBS has emerged as the major pathogen that causes neonatal sepsis and meningitis, and is associated with important morbidity and mortality.[122] Depending on the age of the subject at the time of the manifestation can be divided the disease into two categories: early-onset disease (EOD) and late-onset disease (LOD).[123] The first one is caused by vertical transmission through colonized mother during or just before birth. In fact, GBS can be present in the amniotic fluid and can colonize the fetal skin or mucus membranes or the infant can be exposed to GBS during the passage in the birth canal. Babies are more vulnerable to infection as their immune system cannot fight off the bacteria. In absence of any intervention 50% of the baby born to colonized mother are colonized and 1-2% develop the disease.[124,125] The late-onset disease occur at 7-89 days of life and requires adhesion of GBS to mucosal surfaces and the entry to the bloodstream. Meningitis is one of the late-onset diseases with a consequently risk of long-term neurologic sequelae. [126,127,128,129]

3.1.1 Invasiveness and distribution of different serogroups

Group B Streptococcus (GBS) are covered with a capsular polysaccharide (CPS), that is the major virulence factor of the bacteria and characterize the different serogroup of GBS. Each CPS consist of variously combination of different monosaccharides (usually Gal, Glc and GlcNAc) and a sialic acid residue on the terminal branch of the repeating unit (Fig 3.11). The different structures show differences in linkage position and anomeric configuration while have great similarities in the monosaccharides composition (Fig 3.1.1).[123,130]
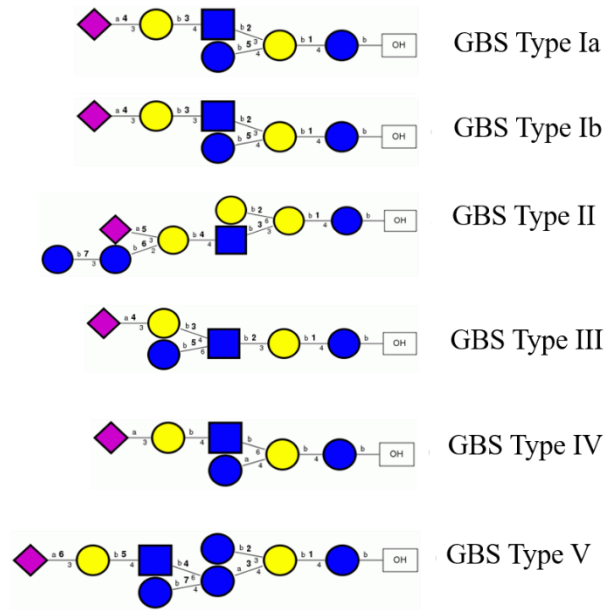
Figure 3.1.1 *Simplified structure of the GBS types Ia, Ib, II, III, IV and V.*

Nine capsular types have been identified Ia, Ib and II-VIII. Among those, serotypes Ia, Ib, II, III, and V are the most invasive in all geographic regions (Table 3.1.1). In particular, studies showed that serotype III accounted for almost 50% of all isolated from infants aged <90 days followed by serotypes Ia, Ib, II, and V. The serotypes Ia, Ib, II, III and V represent for more than 85% of serotypes present in all regions with available data.[121,123]

The ratio of the serotypes isolated from the infants are different than the ones isolated from the colonized mothers. Serotype distribution in colonized mothers may not associate directly with serotypes causing invasive neonatal illness, because the invasiveness seems to be different in the different serogroups. A recent study showed that serotype III (>30%), Ia and V (>20%) were the most frequently isolated in the sub-Saharan Africa[131] while the serotype II (24%) was the most frequently isolated in the region between Thai-Myanmar followed by Ia, VI, III and V. In general, a multi-country study showed that the serotype III was the most frequently isolated followed by serogroups V and Ia. Overall the GBS global distribution appears very heterogeneous.[132]

Ia	→4βGlc1-4[αNeuNAc2-3βGal1-4βGlcNAc1-3]βGal1→
Ib	→4βGlc1-4[αNeuNAc2-3βGal1-3βGlcNAc1-3]βGal1→
II	→3βGlc1-2[αNeuNAc2-3]βGal1-4βGlcNAc1-3[βGal1-6]βGal1-4βGlc1→
III	→4βGlc1-6[αNeuNAc2-3βGal1-4]βGlcNAc1-3βGal1→
IV	→4αGlc1-4[αNeuNAc2-3βGal1-4βGlcNAc1-6]βGal1-4βGlc1→
V	→4βGlc1-4[αNeuNAc2-3βGal1-4βGlcNAc1-6]αGlc1-4[βGlc1-3]βGal1→

Table 3.1.1 *Idealized structures of the repeating units of the six group B Streptococcus polysaccharides responsible of epidemics.*

3.1.2 Treatment

In order to prevent the vertical transmission and the colonization of the newborn, the administration of intravenous ampicillin or penicillin during labor to mother have an efficacy of more than 80% at preventing invasive EOD GBS disease.[133,134] Because not every women are colonized, the universal prophylaxis of all births isn't an optimal strategy, particularly since antibiotic exposure is associated with low but non-zero risks both for the mother and for the baby.[135]

The better solution seems to be the development of specific vaccines to prevent the neonatal GBS diseases. The maternal immunization rather than the direct vaccination of newborns is required to prevent the neonatal and young infant illness. After the maternal immunization the maternal IgG are transmitted transplacentally to the baby [136], and can protect him from the GBS infection. [137,138]

3.1.3 Vaccination - state of the art

Although several vaccines to prevent GBS are in development, none is currently available.

The polysaccharide vaccine is ineffective due to its poor immunogenicity, but the immunogenicity of the CPS conjugate with a carrier protein may be able to induce a stronger and higher functional IgG response.[139,140]

Novartis has developed a trivalent (Ia, Ib and III) CRM_{197} conjugate vaccine and conducted a phase Ib/2 clinical trial (NCT01193920) in neonates born to vaccinated women.[141] Pfizer, in 2017 started to evaluate a pentavalent GBS polysaccharide conjugate vaccine targeting Ia, Ib, II, III and V in phase 1 trial (NCT03170609).[140]

The constant changes in the distribution and importance of the different serogroups require the replacement of old serotypes and the addition of the new ones, making the development of effective multivalent vaccines even more difficult.

3.2 Goals

Since structure and function are intrinsically correlated, herein aimed at performing detailed conformational studies to deduce the three-dimensional structures and dynamic features of the GBS Ia, Ib, II, III, IV and V natural polysaccharides. These studies are very important in order to understand the dynamic and conformational behavior of the different serogroups in solution, and the different presentation of the structural components, the branch, and the backbone. This information can help to define a hypothetical model to develop a multivalent vaccine.

For GBS III, we also aimed at defining the role of the sialic acid in maintaining the three-dimensional structure and to explore the molecular recognition features of the interaction between a synthetic GBS III hexasaccharide with its specific mAbs.

The analysis required the establishment of a robust methodology, based on the synergic application of a series of NMR experiments (TOCSY, NOESY, HSQC, STD NMR, and trNOESY) assisted by molecular modelling methods, in particular Molecular Dynamics simulations.

3.3 Results and discussion

3.3.1 Type III *Streptococcus* B

A combination of NMR methods and Molecular Dynamics (MD) simulations was applied to study the conformational and dynamic behavior of the serotype III *Streptococcus* B capsular polysaccharide (GBS III). It consist of a βGlc1-6[αNeu5Ac2-3βGal1-4]βGlcNAc1-3βGal1-4 repeating unit as highlighted in Fig 3.3.1a.

Previous studies indicate that this molecule assumes a regular helix structure in solution and that the presence of the sialic acid is essential for maintaining this organized conformation.[142,143]

Given the improvements in the last few years in the MD simulations, which allow simulations of longer times with considerably lower computational costs, 3μs of MD were performed to study GBS III in presence and absence of the sialic acid moieties (Fig 3.3.1). The conclusions of the computational data were assessed using NMR experiments (TOCSY, NOESY and HSQC).
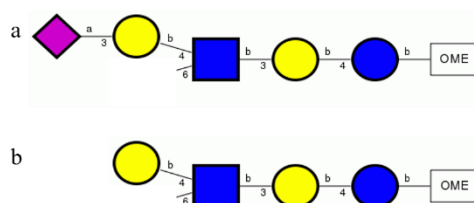
Figure 3.3.1 *Simplified structure of the natural GBS III (a) and the de-sialylated molecule (b) repeat units.*

In addition, the interaction of a synthetic GBS III hexasaccharide with the respective antibody was studied to gain structural insights into this molecular recognition process, using STD-NMR and trNOESY experiments. Indeed previous studies have highlighted that the sialic acid not only has a structural role but is also directly involved in the molecular recognition of the GBSIII CPS by specific antibodies.[144]

3.3.1.1 Molecular Dynamics Simulations

The initial structures for the 7 repeating units of the GBS III polysaccharide, obtained from the GLYCAM-web (Figure 3.3.2). Torsion angles are defined:

ϕ = H1-C1-O-Cx and Ψ = C1-O-Cx-Hx for Gal, Glc and GlcNAc, ϕ_s= C1-C2-O-C3 and Ψ_s= C2-O-C3-H3 for Neu5Ac and ω=O5-C5-C6-O for GlcNAc.

The polysaccharides with and without terminal Neu5Ac (Fig 3.3.2) containing 7 repeating units (DP7) were evaluated to define the conformation around the torsion angles, αNeu5Ac2-3βGal (ϕs) and βGlc1-6βGlcNAc, which involve ω angle. The result of 3μs MD simulation (Fig 3.3.3) reveal that the behavior for every glycosidic bond type is reproducible along the polysaccharide. The analysis showed that the ϕ and ϕs dihedral angles assume a typical *exo-syn* conformation along the entire simulation for both polysaccharides, while there are slight variations around the ψ torsion angles, which are more flexible in the case of the de-sialylated polysaccharide (Fig 3.3.3b). The ω dihedral angles assume predominantly the typical gg (-60°) conformation (Fig 3.3.3).

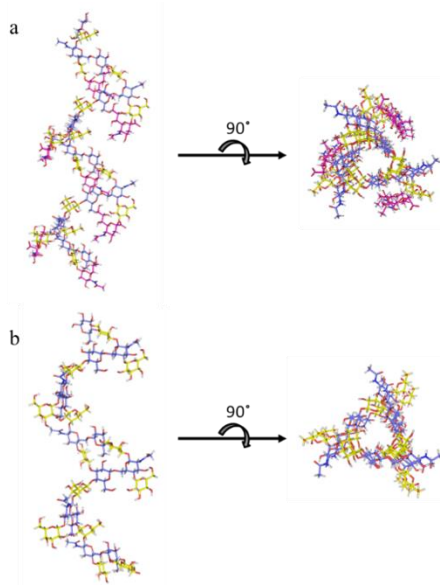*Figure 3.3.2. Representations of the initial structures for the seven repeating unit polysaccharides (a) natural type III and (b) de-sialylated as obtained from the GLYCAM-web, showing the distinct presentation of the outer sialic acid residues*
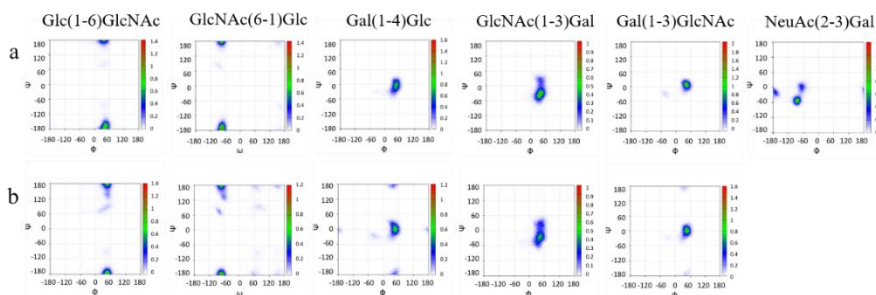
Figure 3.3.3. *Glycosidic linkage analysis for the natural GBS III (a) and de-sialylated (b) polysaccharides: φ/ψ plots for representative glycosidic bonds of a 7 repeating unit model along the 3 µs MD simulation.*

The study of the puckering of the six-membered rings along the long MD permitted to assess that the Gal, Glc and GlcNAc residues assume a typical $^4C_1$ chair during all the simulation, while the Neu5Ac adopt the expected $^1C_4$ geometry.

The global shapes of the entire polysaccharides were also analysed. In particular, the radius of gyration (RoG) was estimated, along with the distances between the non-reducing end moieties with all the other residues (Fig 3.3.4). The RoG describes the overall extension of the molecule and is defined as the root-mean-square distance of the collection of atoms from their common centre of gravity. In this manner, the degree of compactness of the molecule can be deduced in a fairly visual manner. The results show that the behavior of the two molecules in solution is different. In the case of the natural polysaccharide the analysis of the RoG shows a single extended conformation present in solution (Fig 3.3.4-1b). This result is confirmed by the inter-residue distance estimated for the polysaccharide backbone (Fig 3.3.4-1a) that shows that the molecule displays an extended and fairly rigid conformation, with a distance between the non-reducing and reducing end moieties is ca. 70 Å. The analysis of the de-sialylated polysaccharide shows the presence of different conformations in solution, more or less extended (Fig 3.3.4-2b). The distance between the non-reducing and reducing end moieties is ca. 60 Å (Fig 3.3.4-2a), a shorter length than natural GBS III.
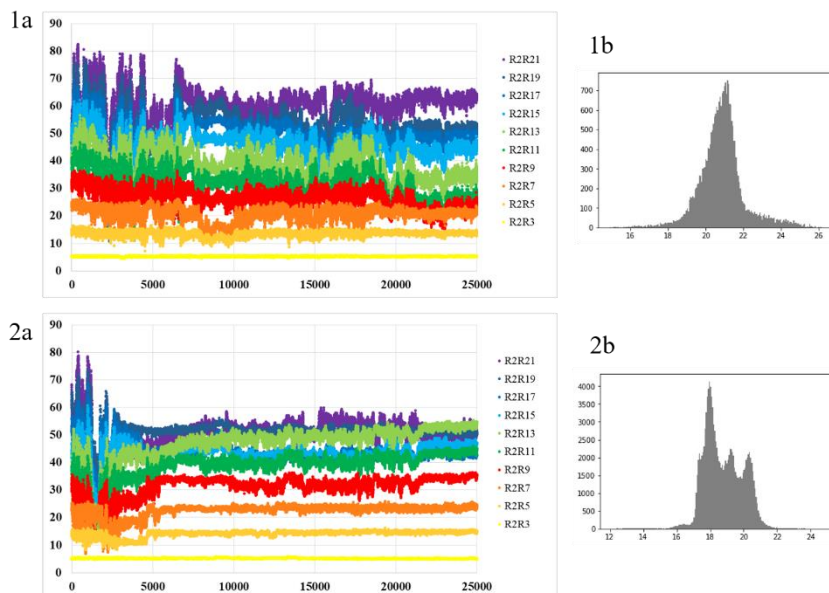
Figure 3.3.4. *Left panels. Calculated inter-residue distances (Å) of the backbone along the MD. From bottom to top: distances between the centre of residue 2 and that of residue 21 (R2−R21) every 2 residues, R2−R19, R2−R17, R2−R15, R2−R13, R2−R11, R2−R9, R2−R7, R2−R5 and R2−R3, respectively for the GBS III (1a) and the GBS III de-salylated (1b) molecules. Right panels. Histograms of the calculated radius of gyration (RoG) of the backbone respectively for GBS III (1b) and GBS III de-sialylated (2b).*

The behavior of ten-repeating unit (DP10) polysaccharides, with and without terminal Neu5Ac, was also investigated. The results confirm the importance of the sialic acid in maintaining the three dimensional helix structure. The natural polysaccharide assumes a regular and well-defined structure during all the simulation, while the conformation of the de-sialylated molecule is irregular and variable, with greater flexibility during the dynamics (Fig 3.3.5).
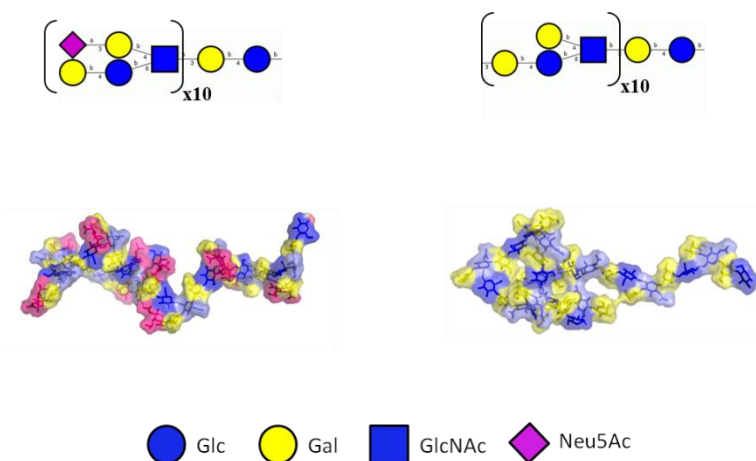
Figure 3.3.5 Snapshot of the most populated structure along the MD simulation for natural GBSIII (left) and de-sialylated (right) DP10. The residues of the backbone are respectively Glc (blue), Gal (yellow) and GlcNAc (light blue) and of the branches Gal (limon) and Neu5Ac (purple).

3.3.1.2 NMR analysis

The theoretical predictions were combined with experimental NMR data and the analysis performed for the polysaccharides was compared with that for a synthetic hexasaccharide containing a single repeating unit (Fig 8). In particular, ^{1}H-^{13}C HSQC and TOCSY (mixing times of 20 and 80ms) experiments were acquired for the poly- and hexasaccharide and NOESY (200ms and 50ms) spectra were acquired for the hexasaccharide and for the polysaccharide respectively. Estimated inter-proton distances from NOESY experiments were compared to those obtained from the MD simulations.

Subsequently the interaction between the hexasaccharide with a specific monoclonal antibody was evaluated by STD-NMR and tr-NOESY experiments in order to identify the epitope involved in the recognition and its conformation.

3.3.1.2.1 Conformational analysis of GBS III

A variety of NMR experiments namely: HSQC, TOCSY (20 ms and 80 ms of mixing time), NOESY (50ms of mixing time) were performed for the natural polysaccharide which permitted to assign its NMR signals (Fig 3.3.6).
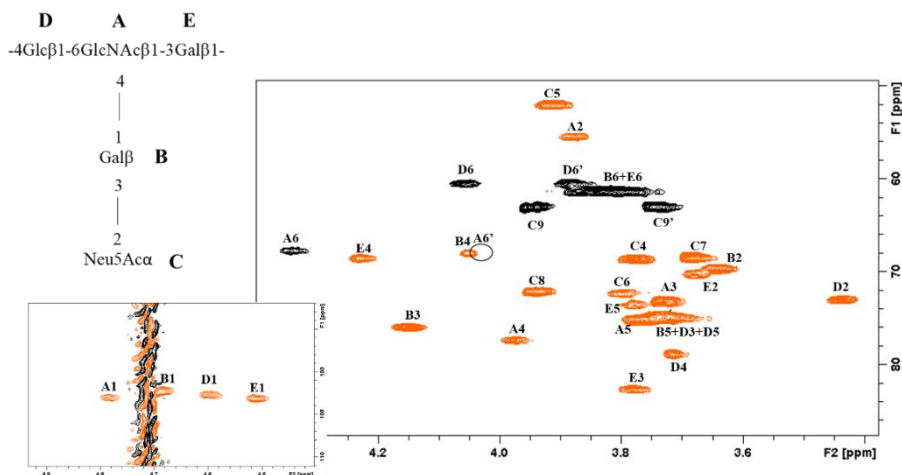
Figure 3.3.6 *^{1}H-^{13}C-HSQC (600MHz, 323K, H$_2$O) of the capsular polysaccharide of GBS III showing the assignment of the ^{1}H and ^{13}C NMR signals.*

Once the NMR signals were assigned, NOE-based experiments were carried out to estimate the key proton-proton distances that could be correlated with the presence of a given conformation around the different glycosidic linkages. The spectra were very complex due to a large line broadening and the overlapping of the different signals.

Despite this, it was possible to define some key NOEs that define the conformation around ϕ and ψ (Fig 3.3.7). The analysis of the NOESY spectra showed strong NOEs for H1GlcNAc(A)-H3Gal(E), H1Gal(E)-H4Glc(D), H1Glc(D)-H6GlcNAc(A) and H1Gal(B)-H4GlcNAc(A), proton pairs that permitted to assess the major presence of the exo-*syn* conformation around the ϕ dihedral angles, in agreement with the computational model (Fig 3.3.3).
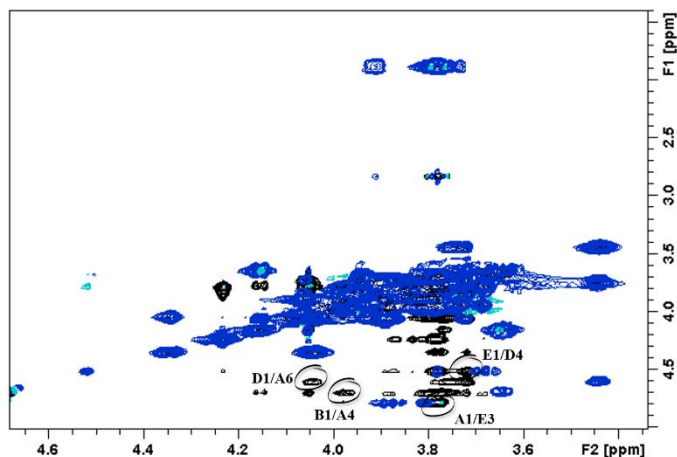
Figure 3.3.7 *NOESY (200 ms mixing time, in black) and TOCSY (20 ms mixing time, in blue) spectra recorded for the CPS of GBSII (800MHz). Key inter-residue NOEs are indicated.*

In the case of the hexasaccharide, HSQC, TOCSY (20 ms and 80 ms of mixing time) and NOESY (200ms of mixing time) were performed and permitted the NMR signal assignment (Fig 3.3.8).
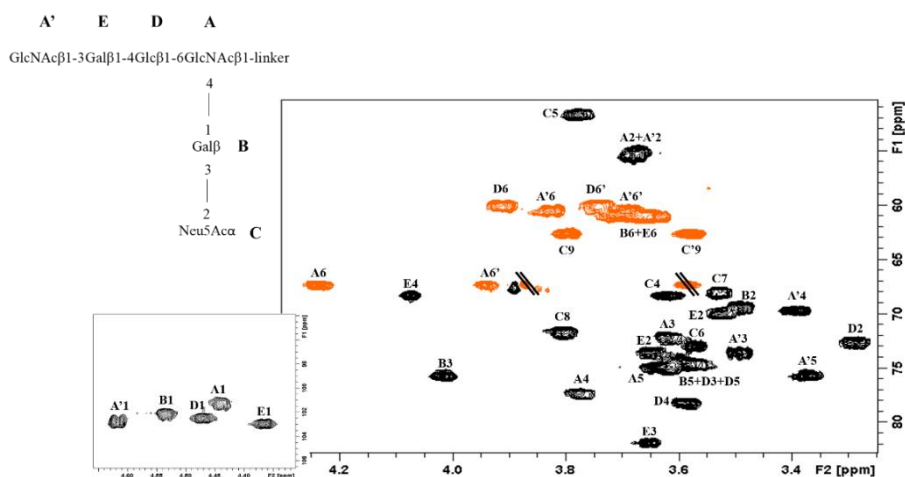
Figure 3.3.8 *^1H-^{13}C-HSQC (600MHz, 298K, D_2O) of the synthetic hexasaccharide of GBS III showing the assignment of the ^1H and ^{13}C NMR signals.*

With respect to interglycosidic flexibility, special attention was payed to the Neu5Acα2-3Gal linkage. According to MD simulations, a conformational

ensemble involving 3 conformers is present for this linkage (Fig. 3.3.9): POP1, where φ/ψ values are ca. 180⁰/-20⁰, and POP2 and POP3, in a close region of the conformational map, with φ/ψ values ca. -90⁰/-50⁰, and -65⁰/-10⁰, respectively.
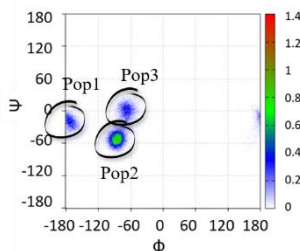
Figure 3.3.9 *φ/ψ plots of αNeu5Ac2-3βGal glycosidic linkage of the GBS III. The three posible conformations are indicated.*

Inter-residue distances were estimated form the intensities of the NOE cross peaks. Experimentally (Fig. 3.3.10 right), the strong H3ax Neu5Ac(C) – H3 Gal(B) NOE yielded an estimated distance of 2.9Å. This value strongly suggests the existence of a conformational equilibrium in solution, with the participation of more than one conformation. Indeed, for POP1 conformation, this distance is below 2.5Å, while for the two other energy minima, POP2 and POP3, this distance is 3.6 Å and 4.2 Å respectively (Table 3.3.1). Additionally, there is a weak NOE between H8 Neu5Ac(C) - H3 Gal(B), which yields an estimated distance of 3.4Å (Fig 3.3.10 left). This distance is around 4.1Å in POP1 and 2.6-2.7Å for POP2 and POP3, corroborating the flexibility around this linkage (Table 3.3.1). Other observed weaker NOEs involving H3 protons of the Neu5Ac residues are H3ax Neu5Ac(C) – H4 Gal(B), H3ax Neu5Ac(C) – H2 Gal(B), H3eq Neu5Ac(C) – H3 Gal(B), H3eq Neu5Ac(C) – H4 Gal(B).

	Pop 1	Pop 2	Pop 3	Experimental
H3Gal – H3eqNeu5Ac	3.6	4.5	4.5	None
H3Gal – H3axNeu5Ac	2.2	3.6	4.2	2.9
H3Gal – H8Neu5Ac	4.1	2.7	2.6	3.4

Table 3.3.1 *Theoretical inter-residue distances of different populations and experimental ones estimated by NMR.*
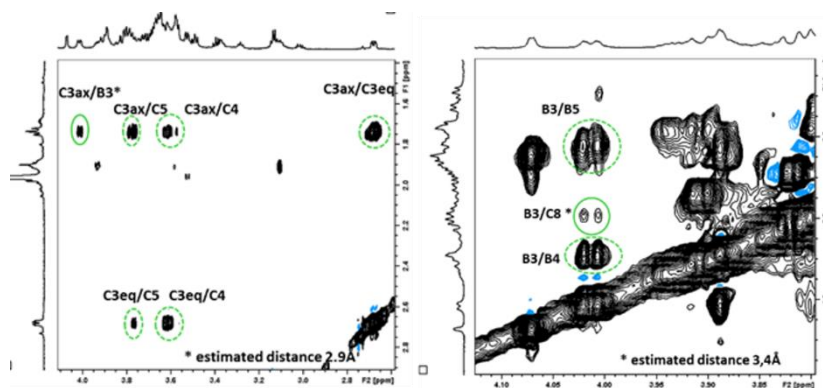
Figure 3.3.10 *NOESY 200 ms mixing time spectrum recorded for the synthetic hexasaccharide of GBSIII. Key inter-residue NOEs are indicated.*

3.3.1.2.2 The interaction of GBS III hexasaccharide to its specific mAbs

The interaction of the hexasaccharide molecule with its specific monoclonal antibody was evaluated by STD-NMR experiments. The analysis of the corresponding experiment for a ca. 1:100 mixture of mAb : hexasaccharide provided strong STD signals.

Two on resonance irradiation frequencies were used, at the aliphatic and at the aromatic regions. Both STD NMR pectra showed clear effects for specific protons of the ligand, and were very similar in terms of relative STD intensities, being in general slighlty larger for the spectrum with aromatic irradiation. The severe signal overlapping in the 3.5-4.1ppm region hampers a detailed epitope mapping (Fig 3.3.8). However, in this region some signals stand out and can be clearly identified as the protons of the NeuAc residue (C). The relative STD intesities for this moiety are represented in the Figure 3.3.11, where it is higlighted that the proton that give the strongest STD intensity is the Acetyl group of the Neu5Ac residue. Additionally, some protons not corresponding to the NeuAc residue can be identified in isolated regions of the STD spectra. The most intense one corresponds to the Acetyl group of the GlcNAc residue(s). The H4 proton of the GlcNAc´residue (A´) also shows weak but clear STD effect.

These results suggest that the main epitope involves the Neu5Ac residue, but the distal GlcNAc´ residue is also close to the protein surface.
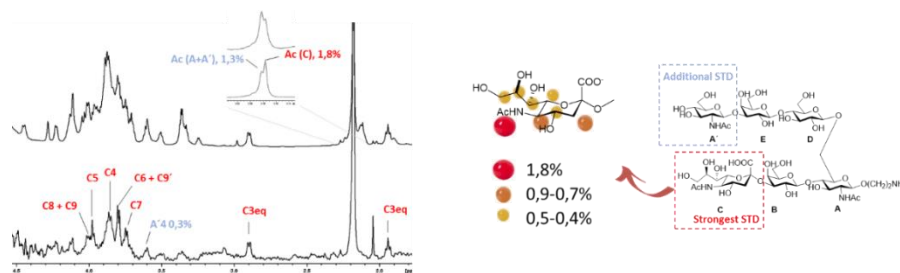
Figure 3.3.11 *¹H-STD-NMR experiment: off-resonance (top) and STD (below) spectra for the hexasaccharide interacting with mAb, with a zoom on N-acetyl signals on the right (left). STD-NMR interpretation: mapping of the hexasaccharide protons more closely interacting with the mAb (right).*

Under the same conditions the spectrum of the hexasaccharide in the presence of the mAb show important changes. Indeed, most of the NOEs of the hexasaccharide are strong and negative, indicating that they are transferred NOES (trNOEs), arising from the mAb-bound conformation. Interestingly, this is not the case for the protons of the aminopropyl moiety (linker), for which the NOEs between their protons are still in the zero NOE region. This clearly indicates that the sugar and the linker moieties of the hexasaccharide present different effective correlation times, as a result of their different interaction with the protein. Thus, in the complex, the linker is pointing far away from the mAb surface and keeps the flexibility of the free-state, while the oligosaccharide´s correlation time is reduced as a result of its interaction with the mAb (Fig 3.3.12).
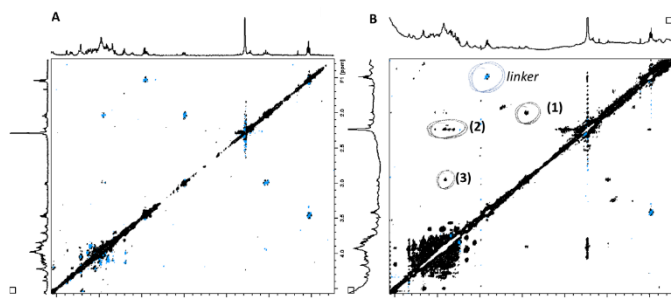
Figure 3.3.12 Comparison of the same regions in the NOESY spectrum of the hexasaccahride free (left) (800MHz) and trNOESY of the hexasaccharide in the presence of the mAb (right) (600MHz). The linker signal are indicated.
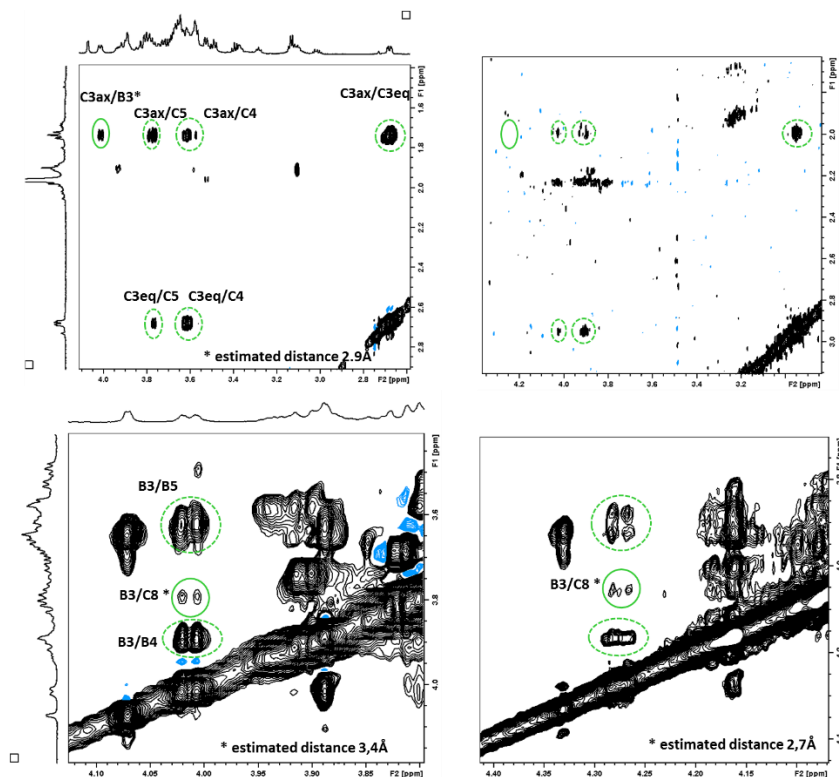
Figure 3.3.13 Comparison of the same regions in the NOESY spectrum of the hexasaccharide free (left) (800MHz) and trNOESY of the hexasaccharide in the presence of the mAb (right) (600MHz).

Interestingly, the situation is different in the trNOESY spectrum (Fig. 3.3.13 left) of the hexasaccharide in the bond state. In this case, the only observable NOEs for H3ax Neu5Ac(C) are the intra-residual ones with H4 and H5, while the inter-residue contacts are absent. On the contrary, the NOE between H3eq Neu5Ac(C) – H4 Gal(B) is more intense in the trNOESY than in the NOESY, yielding an estimated distance for the bound conformation of 2.7 Å.

These information was employed to generate the initial structure of a Molecular Dynamics simulation of the hexasaccharide in the presence of its specific mAb

(pdb 5m63).[144] Figure 3.3.14 shows the different conformation of the αNeu5Ac2-3βGal moiety of the hexasaccharide in the presence and absence of the specific antibody.

These results clearly indicate that there is a conformational selection process around this linkage upon binding. In particular, in the bound conformation, H3-Gal is oriented towards the glycerol chain of the Neu5Ac residue, such as in POP2 and POP3, while the POP1 conformation has disappeared. Although the trNOESY analysis do not permit to quantitatively define the torsion angles, the MD simulation of the hexasaccharide complexed with the mAb shows that the ligand exclusively populates the POP2 region (Fig 3.3.14 right), with a minimum centered at -90º/-50º.
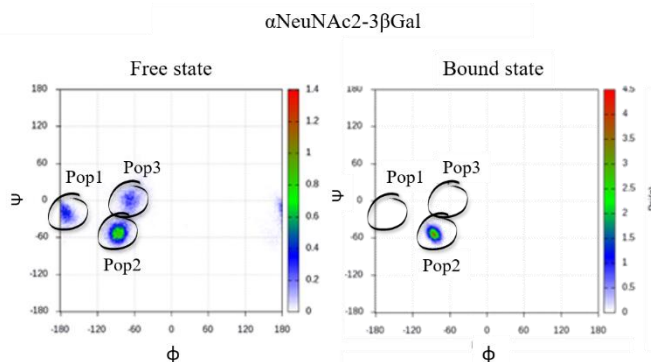
Figure 3.3.14 ϕ/ψ plots for representative αNeu5Ac2-3βGal glycosidic linkage of the GBS III hexasaccharide in free conformation (left) and in the bound state (right).

The result of the MD simulation is shown in Figure 3.3.15A, which also shows the superimposition of different frames of the ligand bound to the mAb. A single frame for the complex is shown in Figure 3.3.15B. The Neu5Ac residue establishes different intermolecular hydrogen bonds with polar amino acid chains at the protein. In particular, the carboxylate group at C1, the carbonyl moiety of NHCOMe at C5, and the hydroxyl group at C4. On the other hand, the Me group of the NHCOMe is buried into a mAb groove and stacked against the aromatic rings of Y52 and Y115 of the light chain. Interestingly, the carbonyl group of the NHCOMe of the GlcNAc A´ residue also establishes hydrogen

bonds with N55 and R66 of the light chain, while the Me group is stacked against Y126 of the heavy chain (Fig. 3.3.15B).
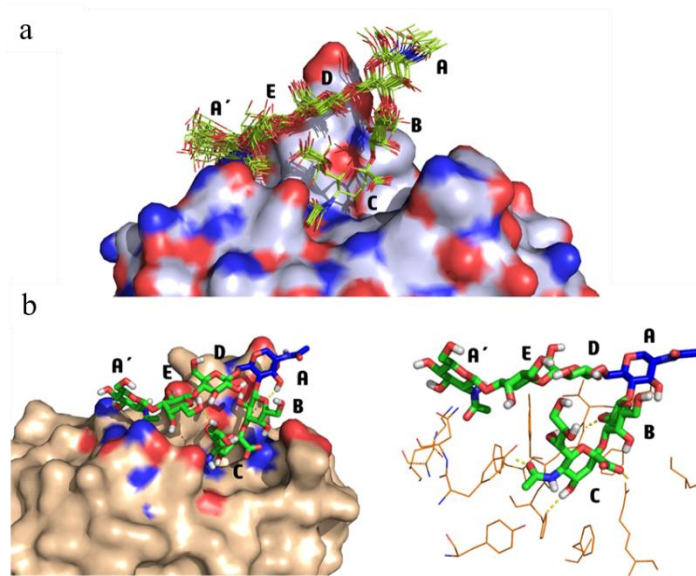
Figure 3.3.15 *(a) Superimposition of different MD frames of the hexasaccharide 1 (in blue) complexed with rabbit Fab (wheat surface), (b) Model for the hexasaccharide 1– rabbit Fab complex from MD simulation.*

3.3.2 Type Ia and Ib *Streptococcus* B

The conformational behavior of the *Streptococcus* B serogroup Ia and Ib capsular polysaccharides (GBS) has been analyzed and compared using a combination of NMR experiments and MD simulations.

The two polysaccharides present a very similar structure. Indeed the repeating unit of the GBS Ia consists of a βGlc1-4[αNeu5Ac2-3βGal1-4βGlcNAc1-3]βGal1-4 while the GBS Ib consists of a βGlc1-4[αNeu5Ac2-3βGal1-3βGlcNAc1-3]βGal1-4. Thus, the two molecules differ only in the linkage between βGal-βGlcNAc in the side chain that is β1-4 in GBS Ia and β1-3 in GBS Ib (Fig 3.3.16).
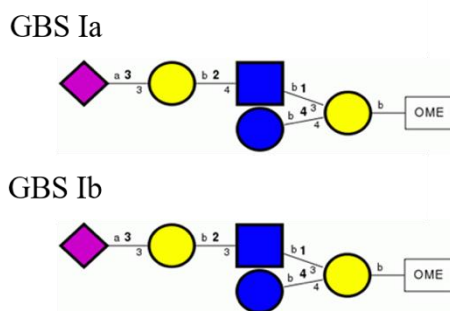
Figure 3.3.16 *Simplified structure of the GBS Ia and Ib repeat units.*

3.3.2.1 Molecular Dynamics simulations

The initial structures of the ten repeating units of the type Ia and type Ib polysaccharides model as obtained from the GLYCAM-web are shown in Figure 3.3.17 and the torsion angles are defined as follows:

φ = H1-C1-O-Cx and Ψ = C1-O-Cx-Hx for Gal, Glc and GlcNAc, φ_s= C1-C2-O-C3 and Ψ_s= C2-O-C3-H3 for Neu5Ac.

After 2.5μs of the MD simulation (GLYCAM06 force field in explicit water), the inspection of the two ensembles allowed defining their three-dimensional

structures and highlighted the effect of the distinct glycosidic linkage between Gal and GlcNAc in their three-dimensional structures.
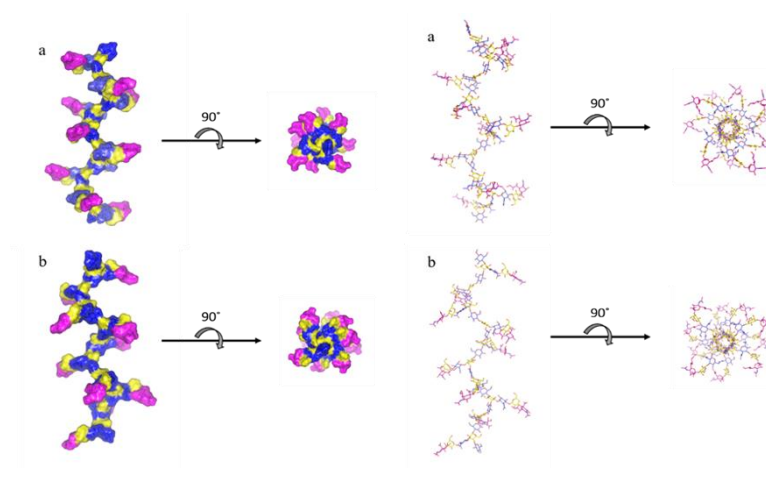
Figure 3.3.17 *Representations of the initial structures for the ten repeating unit polysaccharides (a) type Ia and (b) type Ib as obtained from the GLYCAM web, showing the distinct presentation of the outer sialic acid residues*
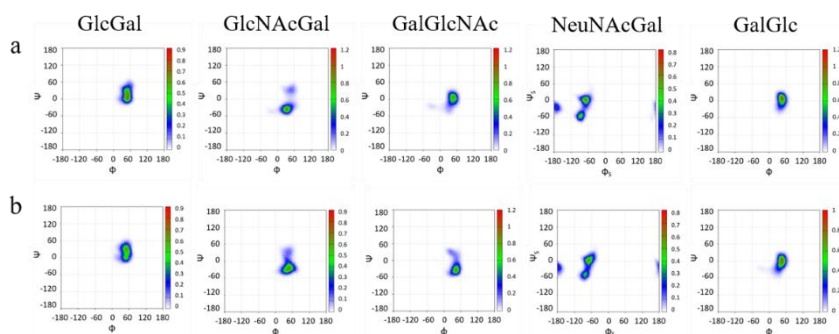
Figure 3.3.18 *Glycosidic linkage analysis for GBS Ia (a) and Ib (b) polysaccharides: ϕ/ψ plots for representative glycosidic bonds of a 10 repeating unit model along the 2.5 µs MD simulation.*

The analysis of the glycosidic linkages was carried out for the 49 glycosidic bonds, revealing that the behaviour for every glycosidic bond type is reproducible along the polysaccharide. Figure 3.3.18 shows a representative analysis for each glycosidic linkage. The Glc1-4Gal, GlcNAc1-3Gal, Gal1-3/4GlcNAc, and Gal1-4Glc linkages populate basically the typical *exo-syn*

conformation for Φ (Fig 3.3.17), while ψ exhibits slightly more flexibility. For the Neu5Ac/Gal linkages, the ϕ_S torsion angles populate both exo-anomeric conformations, the *exo-syn* and the exo-anti. For the *exo-syn* conformation, two populations are differentiated along ψ, which can adopt -60º or 0º values. As stated above, these trends are the same for every repeating unit, regardless of the position in the polysaccharide.

The study of the puckering of the six-membered rings along the long MD permitted to assess that the Gal, Glc and GlcNAc residues assume a typical $^4C_1$ chair during all the simulation, while the Neu5Ac adopt the expected $^1C_4$ geometry.

The global shapes of the entire polysaccharides were also analysed. In particular, the radius of gyration (RoG) was estimated, along with the distances between the non-reducing end moieties with all the other residues (Fig 3.3.19). The RoG describes the overall extension of the molecule and is defined as the root-mean-square distance of the collection of atoms from their common centre of gravity. In this manner, the degree of compactness of the molecule can be deduced in a fairly visual manner.

The results show that the behaviour of the two molecules in solution is fairly similar. In the both cases, a single size population is present in solution. In particular, the inter-residue distance estimated for the polysaccharide backbones show that the molecules display an extended and fairly rigid shapes (Fig 3.3.19 a and c). The computed distances between the non-reducing and reducing-end moieties are ca. 80 Å for the two initial structures and these values is maintained during all the MD run. The RoG analysis show similar conclusions, although Ib seems to be somehow more flexible (Fig 3.3.19d).
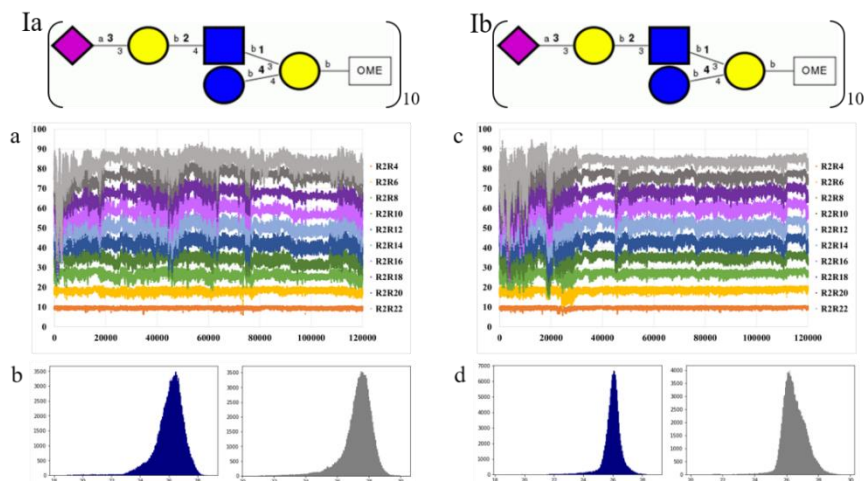
Figure 3.3.19 *Top panels. Representation of the simplified structure of the GBS Ia and Ib polysaccharides employed for the MD simulations. Central panels. Calculated inter-residue distances (Å) of the Glc-Gal backbone along the MD trajectory. From bottom to top: distances between the centre of residue 22 and that of residue 2 (R22−R2) every two residues, R22−R4, R22−R6, R22−R8, R22−R10, R22−R12, R22−R14, R22−R16, R22−R18 and R22−R20, respectively for the GBS Ia (a) and Ib (c) molecules. Bottom panels. Histograms of the calculated radius of gyration (RoG) respectively for GBS Ia (b) and GBS Ib (d). The RoG of the backbones is represented in blue, while that calculated for the entire molecules is shown in grey color. There is a good definition of the global shape for the 50-mer polysaccharides, which is somehow more extended (ca. 1 Å) for GBS Ia.*

3.3.2.2 NMR analysis

The analysis performed for the polysaccharides was compared with that for the corresponding single pentasaccharide repeating units. In particular, ^{1}H-^{13}C HSQC and TOCSY (mixing times of 20 and 80ms) experiments were acquired for the poly- and pentasaccharides, while ROESY (mixing time 200ms) and NOESY (200ms, to be done at 20ms) spectra were acquired for the pentasaccharides and for the polysaccharides respectively. Estimated inter-proton distances from NOESY and ROESY experiments were compared to those obtained from the MD simulations.

3.3.2.2.1 Conformational analysis of the GBS Ia

The conformational behaviour of the minimum pentasaccharide repeating unit of GBS Ia was analysed by using NMR and MD simulations.

^{1}H-^{13}C resonance assignment is shown in Figure 3.3.20 left. NOE-based experiments were carried out to estimate the key proton-proton distances that could be correlated with the presence of a given conformation around the different glycosidic linkages and were compared with the corresponding distances predicted by the MD simulation (Table 3.3.2) for the pentasaccharide. The ROESY spectrum of **1** (Fig 3.3.21) showed key unequivocal inter-residue cross-peaks, which allowed defining the conformation around the glycosidic linkages (Fig 3.3.18). In particular, strong NOEs for H1Gal(B)-H4GlcNAc(C), H1Gal(B)-H6GlcNAc(C) and H1Glc(E)-H4Gal(D) and H1GlcNAc(C)-H3Gal(D) proton pairs permitted to assess the major presence of the exo-*syn* conformation around the ϕ torsion angles of the corresponding glycosidic linkages (Fig 3.3.18). For the glycosidic linkage involving the sialic acid moiety (ϕ_S), the presence of a strong NOE signal (Fig 3.3.21) between H3Gal(B)-H3$_{ax}$Neu5Ac(A) indicated the existence of a major exo-anti (180°) conformation (Fig 3.3.18), but the presence of a weak H3Gal(B)-H8Neu5Ac(A) NOE (Fig 3.3.21) also showed that the *exo-syn* (-60) geometry also participates in the conformational equilibrium (Fig 3.3.18). A view of the major and minor conformations deduced for the GBS Ia pentasaccharide is given in Figures 3.3.22, respectively. Fittingly, these experimental NMR data are in agreement with the computational results obtained through MD simulations for every pentasaccharide repeating unit of the polysaccharide although the exo-anti conformation is underestimated during the simulation.

	MD Penta 500ns	MD Poly 2,5us	Experimental*	180/ -30	-60/0	-60/-50
H3Gal-H3eqNeuNAc	4,2	4,3	none	3,4	4,4	4,6
H3Gal-H3axNeuNAc	3,6	3,7	2.7	2,1	4,3	4,0
H3Gal-H8NeuNAc	3,9	3,9	Very weak	4,8	3,7	3,4
H1Gal-H4GlcNAc	2,4	2,4	2.4			
H1Gal-H6GlcNAc	3,0	3,1	2.7			
H1Gal-H6bGlcNAc	3,9	3,9	3.1			
H1Glc-H4Gal	2,5	2,5	2.6			
H1GlcNAc-H3Gal	2,4	2,4	2.5			

Table 3.3.2 *(Left) Comparison with the key proton-proton distances predicted by MD simulation of the pentasaccharide, polysaccharide and the experimental ones estimated with ROESY experiment for GBS Ia pentasaccharide. (Right) theoretical proton-proton distances in the three major conformations.*

Figure 3.3.20 *(a) ¹H-¹³C-HSQC (600MHz, 298K, D₂O) of the pentasaccharide repeating unit of GBS Ia showing the assignment of the ¹H and ¹³C NMR signals; (b) ¹H-¹³C-HSQC (800MHz, 318K, D₂O) of the GBS Ia CPS showing the assignment of the ¹H and ¹³C NMR signals.*

Figure 3.3.21 ROESY spectrum (200 ms mixing time, in black) and TOCSY (80 ms mixing time, in blue) of the pentasaccharide repeating unit of of GBS Ia (600MHz). Key inter-residue NOEs are indicated.

Figure 3.3.22 Perspectives of the two populations deduced by ROESY NMR experiments that define the conformational behaviour of the pentasaccharide repeating unit of GBS Ia. (Left) the ϕ_S torsion angle adopts the t conformation, (Right) the ϕ_S torsion angle shows the -g conformation. The computed interproton distances are given in Table 1.

3.3.2.2.2 Conformational analysis of the GBS Ib

Similarly to GBS Ia, the conformational behaviour of the minimum pentasaccharide repeating unit of GBS Ib was analyzed by using NMR experiments and compared to the results obtained through the MD simulations carried out for the polysaccharides. In particular HSQC (Fig 3.3.23), TOCSY (mixing times of 20 and 80ms), and ROESY (mixing time 200ms) experiments were acquired for the GBS Ib sample.

Once the NMR signals were assigned, NOE-based experiments were carried out to estimate the key interproton distances that could be correlated with the presence of a given conformation around the different glycosidic linkages, by comparison with the corresponding distances (Table 3.3.3) predicted by MD simulations carried out for the 50-mer polysaccharide. The ROESY spectrum of the pentasaccharide (Fig 3.3.24) showed key unequivocal inter-residue cross-peaks, which allowed defining the conformation around the glycosidic linkages (Fig 3.3.18). In particular, strong NOEs for H1Gal(B)-H3GlcNAc(C) and H1Glc(E)-H4Gal(D) proton pairs permitted to assess the major presence of the

exo-*syn* conformation around the ϕ torsion angles of the corresponding glycosidic linkages (Fig 3.3.18). For the glycosidic linkage involving the sialic acid moiety (ϕ_S), the presence of a NOE signal (Fig 3.3.24) between H3Gal(B)-H3$_{ax}$Neu5Ac(A) indicated the existence of a major t (180°) conformation (Fig 3.3.18), but the presence of a very weak H3Gal(B)-H8Neu5Ac(A) NOE (Fig 3.3.24) showed that also the –g (-60) geometry participates in the conformational equilibrium (Fig 3.3.18). A view of the major and minor conformations deduced for the GBS Ib pentasaccharide is given in Figures 3.3.25, respectively. Fittingly, these experimental NMR data are in agreement with the computational results obtained through MD simulations for every pentasaccharide repeating unit of the polysaccharide although the t conformation is underestimated during the simulation.

	MD Penta 200ns	MD Poly 2,5us	Experimental	180/ -30	-60/0	-60/-50
H3Gal-H3eqNeuNAc	4.3	4,3	None	3,4	4,4	4,6
H3Gal-H3axNeuNAc	3.8	3.8	2.8	2,1	4,4	4,0
H3Gal-H8NeuNAc	3,9	3,8	Very weak	4,8	3,9	3,5
H1Gal-H3GlcNAc	2,4	2,4	2.3			
H1Gal-H2GlcNAc	4.0	4.4	3.4			
H1Glc-H4Gal	2,5	2,7	2.5			
H1GlcNAc-H3Gal	2,5	2,4	overlapped			

Table 3.3.3 *(Left) Comparison with the key proton-proton distances predicted by MD simulation of the pentasaccharide, polysaccharide and the experimental ones estimated with ROESY experiment for GBS Ib pentasaccharide. (Right) theoretical proton-proton distances for the three major conformations.*
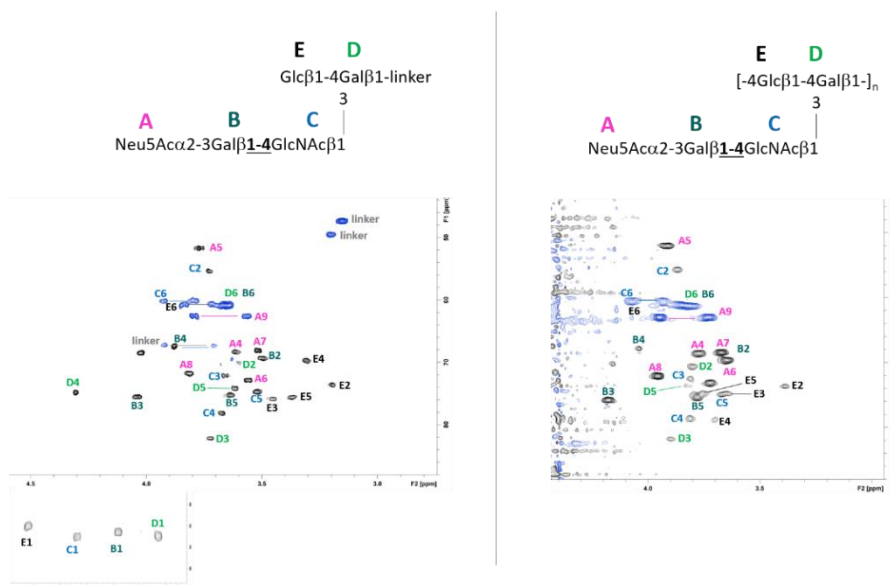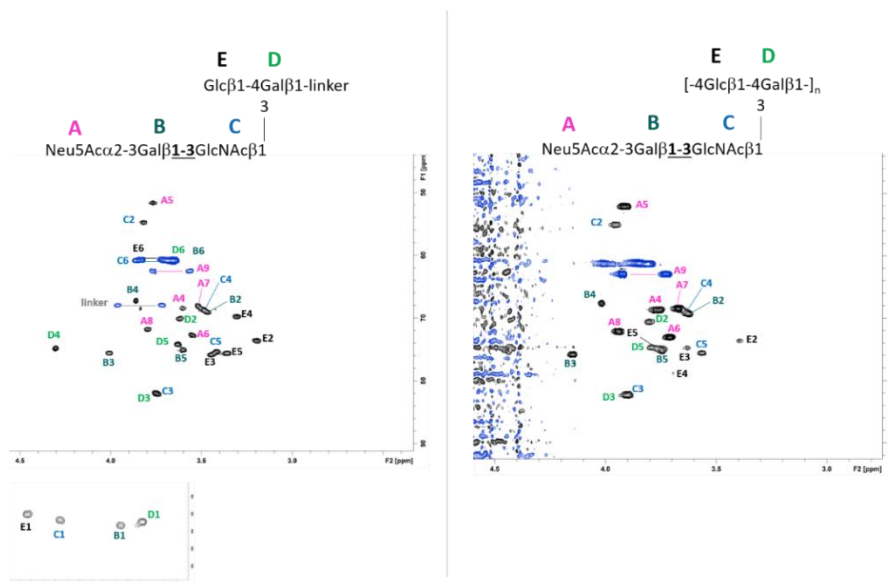
Figure 3.3.23 *(a) ¹H-¹³C-HSQC (600MHz, 298K, D₂O) of the pentasaccharide repeating unit of GBS Ib showing the assignment of the ¹H and ¹³C NMR signals; (b) ¹H-¹³C-HSQC (800MHz, 318K, D₂O) of the GBS Ib CPS showing the assignment of the ¹H and ¹³C NMR signals.*
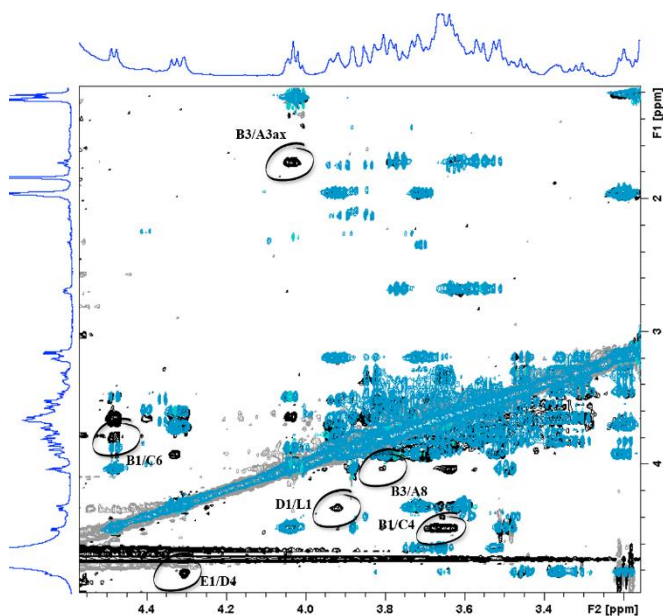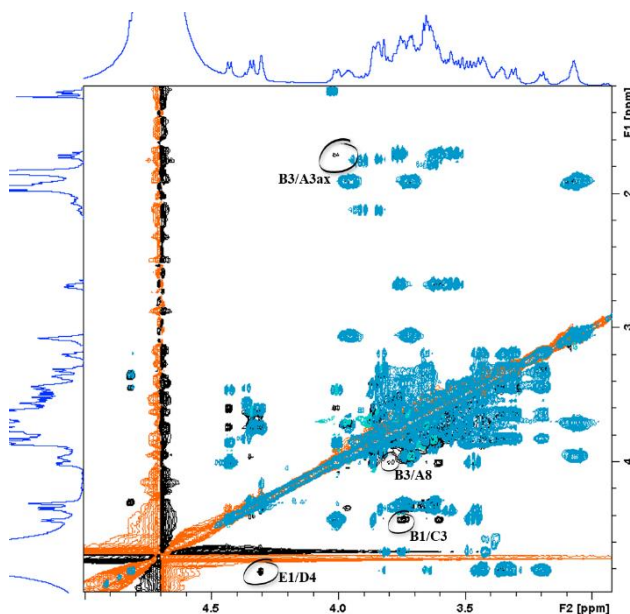

Figure 3.3.24 *ROESY spectrum (200 ms mixing time, in black) and TOCSY (80 ms mixing time, in blue) of the pentasaccharide repeating unit of of GBS Ib (600MHz). Key inter-residue NOEs are indicated.*
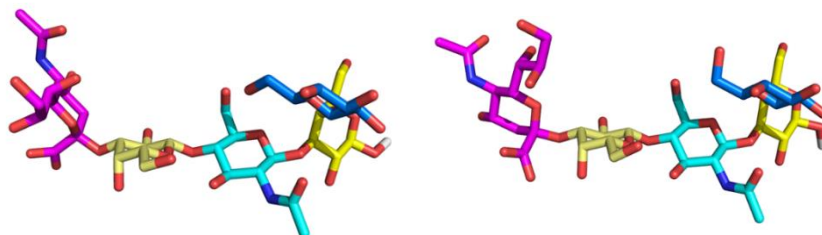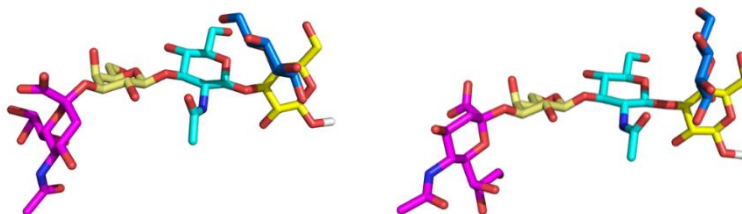
Figure 3.3.25 *Perspectives of the two populations deduced by ROESY NMR experiments that define the conformational behaviour of the pentasaccharide repeating unit of GBS Ib. (Left) the ϕ_S torsion angle adopts the t conformation, (Right) the ϕ_S torsion angle shows the -g conformation. The computed proton-proton distances are given in Table 2.*

3.3.2.2.3 Comparison of the three-dimensional structure of GBS Ia and Ib

The analysis of GBS type Ia and Ib shows that the HSQC spectra of the polysaccharide and the pentasaccharide were very similar, with the obvious exception for the Glcβ1-4 linked moiety (E), which is not glycosylated at O4 in the pentasaccharides (Fig 3.3.20 and 3.3.23).

The comparison of the interglycosidic NOEs shows that the only discrepancies arose again for the Neu5Acα2-3Gal linkages. Interestingly, for the Ia polysaccharide, the NOE-derived distance for H3axNeu5Ac-H3Gal is 2.4Å, shorter than that in the pentasaccharide. At the same time, there is a clear NOE between H3eqNeu5Ac-H3Gal, not observed for the pentasaccharide. On the contrary, for the Ib polysaccharide the distance H3axNeu5Ac-H3Gal is longer, 3.3Å, while the NOE between H3eqNeu5Ac-H3Gal does not exist (Fig 3.3.26 a and b). At the same time, the distance H8Neu5Ac-H3Gal is slightly shorter for the Ib than for the Ia polysaccharide (Fig 3.3.26 c and d).
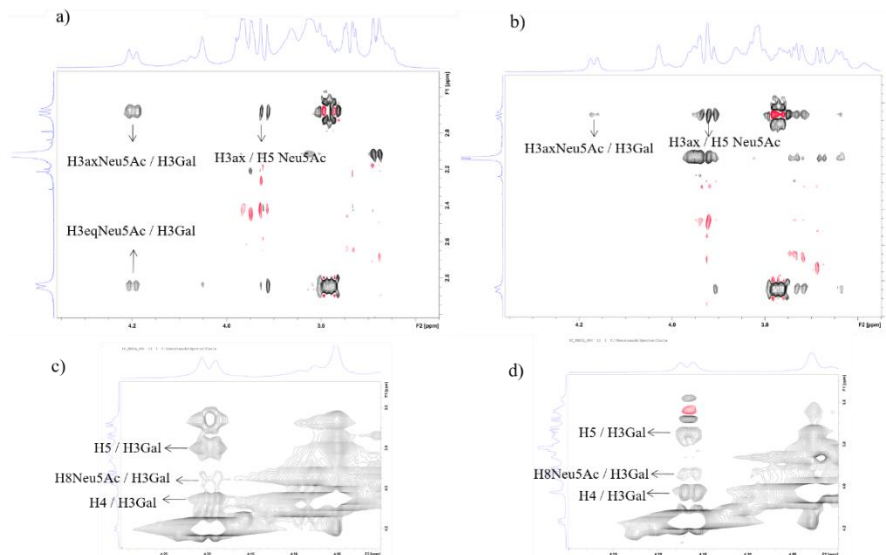
Figure 3.3.26 *The key regions of the NOESY spectra recorded for the GBS Ia (a and c) and GBS Ib (b and d) polysaccharides showing the essential inter residue cross peaks.*

These data suggest that for the Ia polysaccharide, the major conformation around the Neu5Acα2-3Gal fragment is the *exo-anti* (ca. 85%), while for the Ib polysaccharide, there is a larger flexibility, with a major *exo-syn* form (ca. 55%). The model structures for the polysaccharides with all Neu5Acα2-3Gal linkages in *exo-anti* (Ia) and *exo-syn* (Ib) are displayed in Figure 3.3.27, showing different preferential shapes for the two polysaccharides.
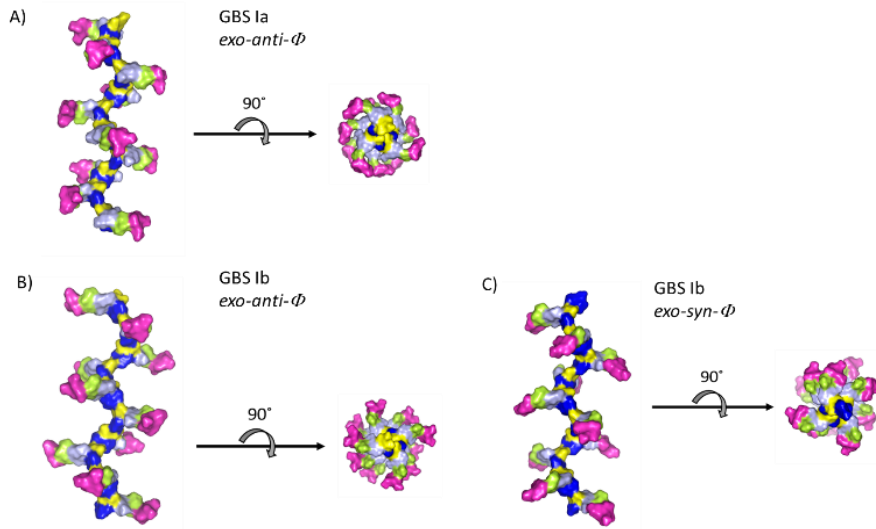
Figure 3.3.27 *Model structures for the GBS Ia and Ib polysaccharides: A) Ia with the major exo-anti conformation around all the Neu5Acα2-3Gal linkages B) Ib with exo-anti conformation around all Neu5Acα2-3Gal linkages and C) Ib with the major exo-syn conformation around all Neu5Acα2-3Gal linkages.*

Capítulo 3.3.3 a 3.4 (ambos inclusive) sujetos a confidencialidad por la autora

3.5 Methods

3.5.1 Molecular Dynamics Simulations. Molecular Dynamics (MD) simulations were performed as described in chapter 2 In this case, long MD simulations between 500 ns and 3 μs were employed to access to the conformational and dynamic information of the molecules.

3.5.2 NMR spectroscopy

The NMR experiments for the polysaccharides were acquired with a Bruker Avance 800 MHz spectrometer equipped with cryoprobe head at 318 K. NMR samples were prepared dissolving 1 mg of material in 500 μL of H_2O/D_2O. The NMR spectra for the penta- (GBS Ia and Ib) and hexa-saccharides (GBS III) were acquired at 298 K on a Bruker Avance 600 MHz spectrometer equipped with PATXI probe. Standard Bruker pulse sequences were used for assignment of the for ^{1}H and ^{13}C resonances.

In particular, for the *GBS Ia and Ib polysaccharides*: [1]H-TOCSY (20 ms and 80 ms mixing times), [1]H-NOESY (20 ms mixing time), ^{13}C-^{1}H HSQC. All experiments employed 512 t1-increments of 4 K points (2 K point for HSQC), with a relaxation delay of 1 s. The ^{1}H dimensions were 8 ppm in TOCSY and NOESY and 7 in HSQC. The ^{13}C dimension was set to 140 ppm. 64 scan were employed for the NOESY, TOCSY, and HSQC. For the GBS Ia and Ib pentasaccharides: [1]H-TOCSY (20 ms and 90 ms mixing times), [1]H-ROESY (200 ms mixing times), ^{13}C-^{1}H HSQC. All experiments employed 256 t_1-increments of 2 K points each, with a relaxation delay of 1 s. The ^{1}H dimensions were 10 ppm. The ^{13}C dimension was 140 ppm.

For the GBS III polysaccharide: [1]H-TOCSY (20 ms and 80 ms mixing times), [1]H-NOESY (200 ms mixing time), ^{13}C-^{1}H HSQC. All experiments employed 256 t_1-increments of 4 K points (2 K point for HSQC), with a relaxation delay of 1 s. The ^{1}H dimensions were always 10 ppm. The ^{13}C dimension was 140 ppm. For the hxasaccharide: [1]H-TOCSY (20 ms and 90 ms mixing times), [1]H-NOESY

(100 ms mixing time), ^{13}C-^{1}H HSQC. All experiments employed 256 t_1-increments of 2 K points, with a relaxation delay of 1 s. The ^{1}H dimensions were always 10 ppm. The ^{13}C dimension is 140 ppm.

For GBS II: ^{1}H-TOCSY (20 ms and 80 ms mixing times), ^{1}H-NOESY (100 ms mixing time), ^{13}C-^{1}H HSQC. All experiments employed 256 t_1-increments of 2 K points, with a relaxation delay of 1 s. The ^{1}H dimensions were always 10 ppm. The ^{13}C dimension was 140 ppm. Due to the high spin diffusion a NOESY (50 ms of mixing time) was also acquired at 318 K with Bruker Avance 600 MHz spectrometer equipped with cryoprobe head.

For GBS IV: ^{1}H-TOCSY (20ms and 70ms of mixing time), ^{1}H-NOESY (100ms of mixing time), ^{13}C-HSQC. All experiments employed 256 t_1-increments of 2 K points, with a relaxation delay of 1 s. The ^{1}H dimensions were 7 ppm. The ^{13}C dimension is 120 ppm. In addition, due to the observed high spin diffusion, a NOESY (50 ms mixing time) was also acquired at 318 K with a Bruker Avance 600 MHz spectrometer equipped with a cryoprobe head.

For GBS V: ^{1}H-TOCSY (20 ms and 80 ms mixing times), ^{1}H-NOESY (100 ms mixing time), ^{13}C-^{1}H HSQC. All experiments employed 256 t_1-increments of 2 K points, with a relaxation delay of 1 s. The ^{1}H dimensions were always 10 ppm. The ^{13}C dimension was 140 ppm. Due to the high spin diffusion additrional NOESY (20 ms and 50 ms of mixing time) were also acquired at 318 K, in D_2O, in a Bruker Avance 600 MHz spectrometer equipped with PATXI probe.

STD-NMR experiments for GBSIII

The mAbs were exchanged in the working buffer (Tris d_{11} 50 mM in D_2O at pH 8.0 +/- 0.1) through a 2 mL Zeba Spin desalting column saturated with 3 cycles of working buffer. The mAbs were finally eluted at the same starting concentration of 1 mg/ml. The 100% of recovery was assessed through microBCA spectrophotometric assay. The hexasaccharide fragment was

desalted, quantified, dried, and then dissolved in the working buffer. For the STD NMR experiments of the hexasaccharide 11 μM of the GBSIII antibody was used in 20 mM PBS buffer in D_2O and pH 7 with a 100:1 ligand/antibody molar ratio.

The STD NMR experiment was carried out at 318 K on a Bruker 800 MHz NMR instrument equipped with cryoprobe. Data acquisition and processing were performed using TOPSPIN 3.5 software, respectively. Suppression of the water signal was achieved by excitation sculpting (2 ms selective square pulse). The protein saturation was achieved by using a Gaussian shape pulse of 50 ms, with a total saturation time of 2 s at frequencies of 7.2 and 0.4 ppm (2 different spectra recorded for the sample). No differences were observed in the STD spectra irradiating at 7.2 or 0.4 ppm for all samples. To avoid pitfalls in the interpretation of the STD-NMR spectra, a negative control spectrum was always recorded in absence of mAb (ligand and buffer) at the same conditions (concentration and pH) of the mAb-saccharide samples. Increasing saturation times from 0.5 up to 4.0 sec were applied to avoid overseeing of possible bias in the calculation of STD effects due to the different proton longitudinal relaxation times (T_1), as well as to the presence of intramolecular spin diffusion within the bound state.

trNOESY

First, NOESY experiments were performed for the hexasaccharide in the free at 600 MHz (200 and 400 ms mixing times) and at 800 MHz (200 and 600 ms mixing times). A 2D-ROESY experiment was also acquired at 600 MHz (200 ms mixing time).

For the bound state, trNOESY experiments were acquired for a sample containing 11 μM of mAb and 20 molar equivalents of hexasaccharide at 600 MHz (100, 200 and 400 ms mixing times) and at 800 MHz (200 ms mixing times).

Contribution to congresses and publications

Oral and Flash communications

Flash presentation: ''Neisseria meningitidis A Capsular Polysaccharide and Carbasugar analogue: Conformational Studies'', 29th International Carbohydrate Symposium, 14th-19th July 2018, Lisboa, Portugal.

Oral presentation: ''Conformational Studies of Neisseria meningitidis A Capsular Polysaccharide and Carbasugar mimetic'', SISOC XII 12th Spanics-Italian Symposium on Organic Chemistry, 2-4 July 2018, Ferrara, Italy.

Seminar: ''Sugar conformation and NMR studies of the interactions of glycan antigens with monoclonal antibodies'' 27 April, 2018. GSK Via Fiorentina, Siena, Italia.

Poster

''Neisseria meningitidis A Capsular Polysaccharide and Carbasugar analogue: Conformational Studies'' Calloni Ilaria, Unione Luca, Corzana Francisco, Jiménez-Osés Gonzalo, Lay Luigi, Adamo Roberto and Jimenéz-Barbero Jesús. 16th Iberian Peptide Meeting 4th ChemBio Group Meeting, 5-7 February 2018, Barcelona, Spain.

''Conformational Studies of Neisseria meningitidis A Capsular Polysaccharide and its mimetics''. Calloni Ilaria, Unione Luca, Corzana Francisco, Jiménez-Osés Gonzalo, Lay Luigi, Adamo Roberto and Jimenéz-Barbero Jesús. 19 th European Carbohydrate Symposium, 2-6 July 2017, Barcelona, Spain.

''Conformational studies of Neisseria meningitidis a CPS and potential mimetics''. Calloni Ilaria, Unione Luca, Corzana Francisco, Jiménez-Osés Gonzalo, Lay Luigi, Adamo Roberto and Jimenéz-Barbero Jesús. XXXVI Reunión Bienal de la Real Sociedad Española de Quimica, 25-29 June 2017, Sitges, Spain.

''NMR and molecular modelling studies of Neisseria meningitidis A capsular polysaccharide and mimetics''. Calloni Ilaria, Unione Luca, Corzana Francisco, Jiménez-Osés Gonzalo, Lay Luigi, Adamo Roberto and Jimenéz-Barbero Jesús. 10th "NMR: a tool for biology" Conference, January 30th to February 1st 2017, Paris, France.

"Conformational Studies of Natural and Mimetics of Neisseria meningitidis A Capsular Polysaccharide Fragments." Ilaria Calloni, Luca Unione, Ana Ardá, Francisco Corzana, Luigi Lay, Roberto Adamo, Jesús Jimenéz-Barbero. 6th EuCheMS Chemistry Congress, 11-15 September 2016, Seville, Spain.

"Natural and Mimetics of Neisseria meningitidis A Capsular Polysaccharide fragments: Conformational Study." Luca Unione, Ana Ardá, Francisco Corzana, Luigi Lay, Roberto Adamo, Jesús Jimenéz-Barbero and Calloni Ilaria. SISOC XI 11th Spanish-Italian Symposium on Organic Chemistry, 13-15 July 2016, Donostia/San Sebastian, Spain.

"New Mimetics of Neisseria meningitidis A: Conformational Study". Calloni Ilaria, Unione Luca, Ardá Ana, Corzana Francisco, Lay Luigi, Adamo Robertod and Jesús Jimenéz-Barbero.8th GERM-5th IBERIAN NMR Meeting, 27-29 June 2016, Valencia, Spain.

Publications

''Structural-guided design of a Group B Streptococcus type III synthetic glycan-conjugate vaccine'' Davide Oldrini, Linda del Bino, Ana Arda, Filippo Carboni, Pedro R. M. Henriques, Francesca Angiolini, Jon I. Quintana, **Ilaria Calloni**, Maria R. Romano, Francesco Berti, Jesus Jimenez-Barbero, Immaculada Margarit, Roberto Adamo. *Chem. Eur. J.* **2020**.

''Regioselective glycosylation strategies for the synthesis of Group Ia and Ib Streptococcus related glycans enable elucidating unique conformations of the capsular polysaccharides'' Linda Del Bino, **Ilaria Calloni**, Davide Oldrini, Maria Michelina Raso, Rossella Cuffaro, Ana Ardá, Jeroen D. C. Codée, Jesús Jiménez-Barbero, and Roberto Adamo. *Chem. Eur. J.* **2019**, 25:16277 – 16287

''The Conformation of the Mannopyranosyl Phosphate Repeating Unit of the Capsular Polysaccharide of Neisseria meningitidis Serogroup A and Its Carba-Mimetic'' **Ilaria Calloni**, Luca Unione, Gonzalo Jiménez-Osés, Francisco Corzana, Linda Del Bino, Alessio Corrado, Olimpia Pitirollo, Cinzia Colombo, Luigi Lay, Roberto Adamo and Jesús Jiménez-Barbero. *Eur. J. Org. Chem.* **2018**, 4548–455.

''Glycans in Infectious Diseases. A Molecular Recognition Perspective'' Unione, L.; Gimeno, A.; Valverde, P.; **Calloni, I.**; Coelho, H.; Mirabella, S.; Poveda, A.; Arda, A.; Jiménez-Barbero. *Curr Med Chem.* **2017**, 24, 4057-4080. (Review).

References

[1] ''How Viruses Enter Animal Cells'' Smith A.E., Helenius A. *Science* **2004**; 304, 5668:237-242. b) Rabinovich, G. A.; Toscano, M. A. *Nat. Rev. Immunol.* **2009**, *9* (5), 338–352.

[2] ''Polysaccharide structure dictates mechanism of adaptive immune response to glycoconjugate vaccines'' Sun X., Stefanetti G., Berti F. and Kasper D.L. *PNAS* **2019**; 116 (1) 193-198.

[3] ''Whole-Cell Cancer Vaccines Induce Large Antibody Responses to Carbohydrates and Glycoproteins'' Xia L., Schrump D.S, Gildersleeve J.C. *Cell Chemical Biology* **2016**; 23, 12:1515-1525. b) Kiessling, L. L.; Splain, R. A. *Annu. Rev. Biochem.* **2010**, *79* (1), 619–653.

[4] ''Carbohydrates as T-cell antigens with implications in health and disease'' Sun L., Middleton D.R., Wantuch P.L, Ozdilek A., and Avci F.Y. *Glycobiology*, **2016**; 26, 10:1029–1040.

[5] ''The biological significance of bacterial encapsulation'' Cross A. *Curr. Top. Microbiol. Immunol*. **1990**; 150:87–95

[6] ''The role of bacterial polysaccharide capsules as virulence factors'' Moxon E., Kroll J. *Curr. Top. Microbiol. Immunol*. **1990**; 150:65–85.

[7] ''Bacterial polysaccharides in sickness and health'' Roberts I. *Microbiology* **1995**; 141:2023–31.

[8] ''Role of capsular polysaccharide (CPS) in biofilm formation and regulation of CPS production by quorum-sensing in Vibrio vulnificus'' Lee K-J., Kim J-A., Hwang W., Park S-J., Lee K-H. *Molecular Microbiology* **2013**; 90(4), 841–857.

[9] ''A Role for Exopolysaccharides in the Protection of Microorganisms from Desiccation'' Ophir T., Gutnick D.L. *Appl. Environ. Microbiol*. **1994**; 60, 2:740-745.

[10] ''Capsular Polysaccharides and Their Role in Virulence'' Russell W., Herwald H. *Concepts in Bacterial Virulence. Contrib Microbiol.* Basel, Karger, **2005**, 12:55-66.

[11] ''Neisseria meningitidis: pathogenesis and immunity'' Pizza M. and Rappuoli R. *Current Opinion in Microbiology* **2015**; 23:68-72.

[12] ''The bacterial glycocalyx in nature and disease'' Costerton J.W., Irvin R.T., Cheng K-J. . *Annu. Rev. Microbiol.* **1981**; 35:299–324 23.

[13] '' Conformational Selection of the AGA*IAM Heparin Pentasaccharide when Bound to the Fibroblast Growth Factor Receptor'' Nieto L., Canales A., Gimenez-Gallego G., Nieto P. M., Jimenez-Barbero J., *Chemistry* **2011**; *17*, 11204.

[14] ''Full ^{1}H NMR assignment and detailed O-acetylation patterns of capsular polysaccharides from Neisseria meningitidis used in vaccine production'' Lemercinier X., Jones C. *Carbohydrate Research* **1996**; 296:83-96.

[15] ''A Solution NMR Study of the Interactions of Oligomannosides and the Anti-HIV-1 2G12 Antibody Reveals Distinct Binding Modes for Branched Ligands'' Enriquez-Navas P. M., Marradi M., Padro D., Angulo J., Penades S. *Chemistry* **2011**; *17*, 1547.

[16] ''NMR Spectroscopic Analysis Reveals Extensive Binding Interactions of Complex Xyloglucan Oligosaccharides with the Cellvibrio japonicus Glycoside Hydrolase Family 31 α-Xylosidase'' Silipo A., Larsbrink J., Marchetti R., Lanzetta R., Brumer H., Molinaro A. *Chemistry* **2012**; *18*, 13395.

[17] ''Bacterial polysaccharides: Components'' Lindberg B. **1998**; p 237–273.

[18] ''Relative stability of $^1C_4$ and $^4C_1$ chair forms of β-D-glucose: a density functional study'' Csonkaa G.I., Éliása K., Csizmadia I.G. *Chemical Physics Letters* **1996**; 257, 1-2: 49-60,

[19] ''A General Definition of Ring Puckering Coordinates'' Cremer D. and Pople J. A. *J. Am. Chem. Soc.* **1975**; 97, 6, 1354-1358.

[20] ''Stereographic representation of the Cremer-Pople ring-puckering parameters for pyranoid rings'' Jeffrey G. A. and Yates J. H. *Carbohydr. Res.* **1979**; 74, 319-322.

[21] ''The three-dimensional structures of the pectic polysaccharides'' Pérez S., Mazeau K., Hervé du Penhoat C. *Plant Physiology and Biochemistry* **2000**; 38, 1–2, 37-55.

[22] ''Mechanism of a Chemical Glycosylation Reaction'' Crich D. *Acc. Chem. Res.* **2010**; 43, 8, 1144-1153.

[23] ''Acceptor reactivity in glycosylation reactions'' van der Vorm S., van Hengst J.M.A., Hansen T., Overkleeft H.S., van der Marel G.A. and Codée J.D.C. *Chem Soc Rev*. **2019**; 48(17):4688-4706.

[24] ''Recent advances in reagent-controlled stereoselective/stereospecific glycosylation'' Yao H., Vu M.D. and Liu X.W. *Carbohydr Res*. **2019**; 473:72-81.

[25] (a) Edward J.T. *Chem. Ind. (London)* **1955**; 1102-1104. (b) ''Configurational effects on the Proton Magnetic Resonance Spectra of the Six-membered Ring Compounds'' Lemieux R.U., Kullnig R.K., Bernstein H.J. and Schneider W.G. *J. Am. Chem. Soc.* **1958**, 80, 22, 6098-6105.

[26] ''The origin of the anomeric effect: conformational analysis of 2-methoxy-1,3-dimethylhexahydropyrimidine'' Perrin C.L., Armstrong K.B and Fabian M.A *J. Am. Chem. Soc.* **1994**, 116, 2:715-722.

[27] ''Anomeric and Exo-Anomeric Effects in Carbohydrate Chemistry'' Tvaroŝka I. and Bleha T. *Advances in Carbohydrate Chemistry and Biochemistry* **1989**; 47, 45-123.

[28] (a) ''Further justification for the exo-anomeric effect Conformational analysis based on nuclear magnetic resonance spectroscopy of oligosaccharides'' Thøgersen H., Lemieux R., Bock K. and Meyer, B. *Can. J. Chem.* **1981**; 60, 44–57. (b) Xu, B.; Unione, L.; Sardinha, J.; Wu, S.; Ethève-Quelquejeu, M.; Rauter, A. P.; Blériot, Y.; Zhang, Y.; Martín-Santamaría, S.; Díaz, D.; Jiménez-Barbero, J.; Sollogoub, M. *Angew. Chemie Int. Ed.* **2014**, *53*, 9597–9602.

[29] ''Stereoelectronic and Solvation Effects Determine Hydroxymethyl Conformational Preferences in Monosaccharides'' Barnett C. B. and Naidoo K. J., *J. Phys. Chem. B* **2008**; 112, 15450.

[30] ''NMR Spectroscopy in the Study of Carbohydrates: Characterizing the Structural Complexity'' Bubb W.A. *Concepts in Magnetic Resonance Part A* 2003; Vol. 19A(1) 1–19.

[31] ''Structure and dynamics of oligosaccharides: NMR and modeling studies'' Peters T. and Pinto B.M. *Current Opinion in Structural Biology* **1996**; 6, 5:710-720.

[32] ''Well-Defined Oligo- and Polysaccharides as Ideal Probes for Structural Studies'' Delbianco M. Kononov A., Poveda A., Yu Y., Diercks T., Jiménez-Barbero J. and Seeberger P.H . *J. Am. Chem. Soc.* **2018**, 140, 16, 5421-5426.

[33] ''The Conformation of the Mannopyranosyl Phosphate Repeating Unit of the Capsular Polysaccharide of Neisseria meningitidis Serogroup A and Its Carba-Mimetic'' Calloni I., Unione U., Jiménez-Osés G., Corzana F., Del Bino L., Corrado A., Pitirollo O., Colombo C., Lay L., Adamo R. and Jiménez-Barbero J. *Eur. J. Org. Chem*. **2018**; 4548–4555.

[34] ''High-Resolution NMR Techniques in **Organic Chemistry''** Claridge T. D. W. *Tetrahedron Organic Chemistry Series* **1999**; *19*.

[35] ''Understanding NMR Spectroscopy'' Zheltikov A.; James Keeler, John Wiley & Sons Ltd, Chichester, **2005**, 459, paperback, ISBN: 0470017872.

[36] ''50th Anniversary Perspective: The Importance of NMR Spectroscopy to Macromolecular Science'' Spiess H.W. *Macromolecules* **2017**; 50, 5, 1761-1777.

[37] ''Carbohydrate Structural Determination by NMR Spectroscopy: Modern Methods and Limitations'' Duus J. Ø., Gotfredsen C. H., Bock K. *Chem. Rev.* **2000**; 100, 12, 4589-4614.

[38] ''Unveiling the structure of sulfated fucose-rich polysaccharides via nuclear magnetic resonance spectroscopy'' Mourão P.A.S., Vilanova E., Soares P.A.G. *Current Opinion in Structural Biology* **2018**; 50, 33-41.

[39] ''Exploration of conformational spaces of high-mannose-type oligosaccharides by an NMR-validated simulation'' Yamaguchi T. et al. *Angew. Chemie - Int. Ed.* **2014**; 53, 10941–10944.

[40] ''Structure and conformation of complex carbohydrates of glycoproteins, glycolipids, and bacterial polysaccharides'' Bush C.A., Martin-Pastor M. and Imberty A. *Annual Review of Biophysics and Biomolecular Structure* **1999**; 28:269-293.

[41] ''Protein-carbohydrate interactions studied by NMR: from molecular recognition to drug design.'' Fernandez-Alonso M., C. Diaz D., Berbis A.M., Marcelo F., Cañada J., Jimenez-Barbero J. *Curr. Protein Pept. Sci.* **2012**; 13, 816–30.

[42] ''The recognition of glycans by protein receptors. Insights from NMR spectroscopy'' Ardá A. and Jiménez-Barbero *J. Chem. Comm* **2018**; 38.

[43] ''NMR developments in structural studies of carbohydrates and their complexes'' Van Halbeek H. *Current Opinion in Structural Biology* **1994**; 4, 5, 697-709.

[44] (a)''Contact Electron-Spin Coupling of Nuclear Magnetic Moments'' Karplus M. *J. Chem. Phys.* **1959**; 30, 11.

[45] ''Developments in the Karplus equation as they relate to the NMR coupling constants of Carbohydrates'' Coxon B. *Adv. Carbohydr. Chem. Biochem.* **2009**; 62, 17–82.

[46] ''Insights into furanose solution conformations: beyond the two-state model'' Wang X. and Woods R. J. *J. Biomol. NMR* **2016**; 64, 209-305.

[47] ''Experimental evidence of deviations from a Karplus-like relationship of vicinal carbon-proton coupling constants in some conformationally rigid carbohydrate'' Cano F.H., Foces-Foces C., Jimenez-Barbero J., Alemany A., Bernabe M., Martin-Lomas M. *J. Org. Chem.* **1987**, 52, 15, 3367-3372.

[48] ''New Karplus equations for $^2J_{HH}$, $^3J_{HH}$, $^2J_{CH}$, $^3J_{CH}$, $^3J_{COCH}$, $^3J_{CSCH}$, and $^3J_{CCCH}$ in some aldohexopyranoside derivatives as determined using NMR spectroscopy and density functional theory calculations'' Tafazzoli M. and Ghiasi M. *Carbohydr. Res.* **2007**; 342, 2086–2096.

[49] ''Principles of nuclear magnetic resonance in one and two dimensions'' Ernst R. R., Bodenhausen G., Wokaun, A., Oxford University Press: Oxford, England, **1990**.

[50] ''The nuclear Overhauser effect in structural and conformational analysis'' Neuhaus D., Williamson M. P. Wiley, VCH: New York, USA, **2000**.

[51] ''Spin dynamics: basics of nuclear magnetic resonance'' Levitt M. H.; Wiley: Chichester, England, **2001**.

[52] ''NMR spectroscopy of Glycoconjugates'' Jimenez-Barbero J. and Peters T. *Wiley-VCH* **2003.**

[53] ''NMR Spectroscopy Techniques for Screening and Identifying Ligand Binding to Protein Receptors'' Meyer B. and Peters T. *Angew. Chem. Int. Ed.* **2003**, 42, 8.

[54] ''NMR and molecular recognition. The application of ligand-based NMR methods to monitor molecular interactions.'' Unione L., Galante S., Díaz D., Cañada J. and Jiménez-Barbero J. *MedChemComm.* **2014;** 5, 1280-1289.

[55] ''Intermolecular spin diffusion as a method for studying macromolecule-ligand interactions'' Akasaka K. *Journal of Magnetic Resonance* **1969**; 36, 1, 135-140.

[56] ''Saturation-Transfer Difference (STD) NMR: A Simple and Fast Method for Ligand Screening and Characterization of Protein Binding'' Viegas A., Manso J., Nobrega F.L., and Cabrita E.J. *J. Chem. Educ*. **2011**; 88, 990–994.

[57] ''Conformational Studies of Oligosaccharides and Glycopeptides: Complementarity of NMR, X-ray Crystallography, and Molecular Modelling'' Wormald M.R., Petrescu A.J., Pao Y., Glithero A., Elliott T., and Dwek R.A. *Chem. Rev*. **2002**; 102, 371−386.

[58] ''Biomolecular simulation: a computational microscope for molecular biology.'' Dror R. O., Dirks R. M., Grossman J. P., Xu H. and Shaw D. E. *Annu. Rev. Biophys.* **2012**; 41, 429–52.

[59] ''Molecular dynamics simulations and drug discovery'' Durrant J. D. and McCammon J. A. *BMC Biol.* **2011**; 9, 71.

[60] ''Computational biochemistry and biophysics'' Becker O. M., MacKerel A., Roux B., Watanabe M. *Dekker M, New York* **2001**.

[61] 'Essentials of computational chemistry: theories and models'' Cramer, C. J. *John Wiley & Sons*, **2004**.

[62] Case D., Cerutti D., Cheatham T., Darden T., Duke R., Giese T., Gohlke H., Goetz A., Greene D., Homeyer N., Izadi S., Kovalenko A., Lee T., LeGrand S., Li P., Lin C., Liu J., Luchko T., Luo R., Mermelstein D., Merz K., Monard G., Nguyen H., Omelyan I., Onufriev A., Pan F., Qi R., Roe D., Roitberg A., Sagui C., Simmerling C., Botello-Smith W., Swails J., Walker R., Wang J., Wolf R., Wu X., Xiao L., York D., Kollman P. AMBER 2017. San Francisco, CA: University of California **2017**.

[63] ''GLYCAM06: A Generalizable Biomolecular Force Field. Carbohydrates. Journal of Computational Chemistry'' Kirschner K., Yongye A., Tschampel S., González-Outeiriño J., Daniels C., Foley B.L. and Woods R.. *Journal of Computational Chemistry* **2008**; 29:622-655.

[64] ''Development and testing of a general amber force field.'' Wang J., Wolf R., Caldwell J., Kollman P., Case D. *Journal of Computational Chemistry* **2004**; 25(9):1157-1174.

[65] ''Building Water Models: A Different Approach'' Izadi S., Anandakrishnan R. and Onufriev A.V. *J. Phys. Chem. Lett.* **2014**; 5, 3863−3871.

[66] ''Comparison of simple potential functions for simulating liquid water''.Jorgensen W. L., Chandrasekhar J., Madura J. D., Impey R. W. and Klein M. L. *The Journal of Chemical Physics* **1983**; 79 , 926-935.

[67] ''Molecular dynamics simulations of large macromolecular complexes'' Perilla J.R, Goh C.G, Cassidy C.K., Liu B., Bernardi R.C., Rudack T., Yu H., Wu Z. and Schulten K. *Current Opinion in Structural Biology* **2015**; 31:64–74.

[68] ''Early Experiences Porting the NAMD and VMD Molecular Simulation and Analysis Software to GPU-Accelerated OpenPOWER Platforms'' Stone J.E., Hynninen A., Phillips J.C. and Schulten K. *ISC High Performance 2016: High Performance Computing* **2016**; 188-206.

[69] ''Molecular Dynamics Simulation for All'' Hollingsworth S.A. and Dror R.O. *Neuron* **2018**; 99, 6:1129-1143.

[70] *''Guide to Molecular Mechanics and Quantum Chemical Calculations*.'' Hehre W. J. *A Wavefunction* **2003**.

[71] *''Chemist' s Guide to Density Functional Theory*.'' Koch W. and Holthausen M. C. *A* **2001**.

[72] Gaussian 09, Revision A.02, Frisch M. J., Trucks G. W., Schlegel H. B., Scuseria G. E., Robb M. A., Cheeseman J. R., Scalmani G., Morokuma K., Farkas O., Foresman J. B., and Fox D. J., Gaussian, Inc., Wallingford CT, **2016**.

[73] '' Sensing the anomeric effect in a solvent-free environment.'' Cocinero E. J., Carçabal P., Vaden T. D., Simons J. P. and Davis B. G *Nature* **2011** 469, 76–79.

[74] ''NMR and DFT Analysis of Trisaccharide From Heparin Repeating-Sequence.'' Hricovini M., Driguez P. A. and Malkin O. *J. Phys. Chem. B* **2014**; 118, 11931−11942.

[75] ''Complete assignments of the 1H and 13C chemical shifts and JH,H coupling constants in NMR spectra of D-glucopyranose and all D-glucopyranosyl-D-glucopyranosides.'' Roslund M. U., Tähtinen P., Niemitz M. and Sjöholm R. *Carbohydr. Res.* **2008**; 343, 101–112.

[76] ''Theoretical examination of the S-C-P anomeric effect.'' Juaristi E. and Notario R. *J. Org. Chem.* **2015**; 80, 2879–2883.

[77] ''Proper basis set for quantum mechanical studies of potential energy surfaces of carbohydrates.'' Csonka, G. I. *J. Mol. Struct. THEOCHEM* **2002**; 584, 1–4.

[78] ''Conformational analysis of xylobiose by DFT quantum mechanics'' Ling, J.Z., Edwards V., Nam S., Xu F. and French A.D. *Cellulose* 2019. https://doi.org/10.1007/s10570-019-02874-3.

[79] ''Nasopharyngeal carriage of *Neisseria meningitidis* in general population and meningococcal disease''. Ichhpujani R.L., Mohan R., Grover S.S., Joshi P.R., Kumari S., <u>*J Commun Dis.*</u> **1990** Dec;22(4):264-8.

[80] '*Neisseria meningitidis*: an overview of the carriage state'', Yazdankhah S.P. and Caugant D.A., *Journal of Medical Microbiology* **2004**, 53, 821–832.

[81] Centers for Disease Control and Prevention Meningococcal disease: Technical and clinical information. Available at: http://www.cdc.gov/meningococcal/clinical-info.html. **2017**.

[82] ''Meningococcal disease: Clinical presentation and sequelae'', Pace D. and Pollard A.J.; *Vaccine* (**2012**).

[83] ''Meningococcal disease'', Rosenstein N.E., Bradley M.D. et al, *N Engl J Med* (**2001**), Vol. 344, No. 18 May 3,

[84] ''Meningococcal meningitis in Africa'', Greenwood B., *Transactions of the Royal Society of tropical medicine and hygiene* (**1999**) 93,341-353.

[85] World Health Organization regional office for Africa. Available at: https://www.who.int/news-room/fact-sheets/detail/meningococcal-meningitis (**2018**).

[86] ''Advances in treatment of bacterial meningitis'', Van de Beek D.., Brouwer M.C., Thwaites G.E., Tunkel A.R., *Lancet* (**2012**), 380: 1693–702.

[87] '' Effect of vaccines on bacterial meningitis worldwide'', McIntyre P.B., O'Brien K.L., Greenwood B., Van de Beek D., *Lancet* **2012**; 380: 1703–1.

[88] ''Description and Nomenclature of Neisseria meningitidis Capsule Locus'', O.B. Harrison et al; *Emerging Infectious Diseases*, April **2013**, 19, 4.

[89] ''Molecular divergence of the sia locus in different serogroups of *Neisseria meningitidis* expressing polysialic acid capsules'', Claus H., Vogel U., Muhlenhoff M., Gerardy-Schahn R., Frosch M., *Mol Gen Genet* **1997**, 257: 28-34.

[90] ''Determination of the structure and conformation of bacterial polysaccharides by Carbon 13 Nuclear Magnetic Resonance - studies on the group specific antigens of *Neisseria meningitidis* serogroups A and X'', Bundle D.R., Smith I.C.P. and Jennings H.J.; *The Journal Of Biological Chemistry* **1974**, 249, 2275-2281.

[91] ''Neisseria meningitidis: biology, microbiology, and epidemiology'', Rouphael, N.G.; Stephens D.S.; *Method Mol. Biol*. **2012**, *799*, 1-20.

[92] ''Bioanalysis of meningococcal vaccines'', Ravenscroft N., Wheeler J.X. and Jones C.; *Bioanalysis* **2010**, 2(2), 343–361.

[93] ''Impact of MenAfriVac in nine countries of the African meningitis belt, 2010–15: an analysis of surveillance data''.Trotter C.L., Lingani C., Fernandez K., Cooper L.V., Bita A., Tevi-Benissan C., Ronveaux O., Preziosi M.P., Stuart J.M. *Lancet Infect Dis* **2017** 17:867–872.

[94] ''Successful African introduction of a new Group A meningococcal conjugate vaccine: future challenges and next steps'', LaForce F.M., Djingarey M., Viviani S., Preziosi M.P.; *Hum Vaccin Immunother* **2018***, 14:1098–1102.

[95] ''Safety and immunogenicity of a pentavalent meningococcal conjugate vaccine, containing serogroups A, C, Y, W, and X, in healthy adults: a phase 1, single-centre, double-blind, randomised, controlled study'', Chen W.H., Neuzil K.M., Boyce C.R., et al. *Lancet Infect Dis* **2018**;
[96] ''Meningococcal Group A, C, W and Y Tetanus Toxoid conjugatevaccine: a review of clinical data in adolescents'', Serra L.C., MBiotech, York L.J., Balmer P. and Webber C.; *Journal of Adolescent Health* **2018**, 63, 269-279.

[97] ''Routinely vaccinating adolescents against meningococcus: Targeting transmission & disease.'', Vetter V., Baxter R., Denizer G., et al. *Expert Rev Vaccines* **2016**;15:641–58.

[98]''Relative stability of meningococcal serogroup A and X polysaccharides'', Berti F, Romano MR, Micoli F, Pinto V, Cappelletti E, Gavini M, Proietti D, Pluschkec G,. MacLennan CA, Costantino P; *Vaccine* **2012**, 30, 6409– 6415.

[99] ''Immunoactivity of protein conjugates of Carba Analogues from *Neisseria meningitidis* A capsular polisaccharide'', Gao Q., Tontini M., Brogioni G., Nilo A., Filippini S., Harfouche C., Polito L., Romano M.R., Costantino P., Berti F., Adamo R., and Lay L.. *ASC Chem. Biol*. **2013**, 8, 2561-2567.

[100] ''Synthesis and biological evaluation of phosphono analogues of capsular polysaccharide fragments from Neisseria meningitidis A'', Torres-Sanchez M.I., Zaccaria C., Buzzi B., Miglio G., Lombardi G., Polito L., Russo G., and Lay L.; *Chem. Eur. J.* **2007**, 13, 6623 – 6635.

[101] ''A synthetic disaccharide analogue from *Neisseria meningitidis* A capsular polysaccharide stimulates immune cell responses and induces Immunoglobulin G (IgG) production in mice when Protein-Conjugated'', Fallarini S., Buzzi B., Giovarruscio S., Polito L., Brogioni G., Tontini M., Berti F., Adamo R., Lay L., and Lombardi G.; *ASC Infect. Dis.* **2015**, 1, 487-496.

[102] Woods Group. (2005-2019) GLYCAM Web. Complex Carbohydrate Research Center, University of Georgia, Athens, GA. (http://glycam.org)

[103] a) Mayer, M.; Meyer, B. Group Epitope Mapping by Saturation Transfer Difference NMR To Identify Segments of a Ligand in Direct Contact with a Protein Receptor. *J. Am. Chem. Soc.* **2001**, *123*, 6108-6117.

[104]4JCOCCH and 4JCCCCH as Probes of Exocyclic Hydroxymethyl Group Conformation in Saccharides, Qingfeng Pan, Thomas Klepach, Ian Carmichael, Meredith Reed, and Anthony S. Serianni, *J. Org. Chem*. **2005**, 70, 7542-7549.

[105] A conformational study of hydroxymethyl groups in carbohydrates investigated by 'H nmr spectroscopy, Klaus Bock and Jens Ø. Duus, J. *Carbohydrate Chemistry*, **1994** 13(4), 513-543.

[106] a) Mayer, M.; Meyer, B. Group Epitope Mapping by Saturation Transfer Difference NMR To Identify Segments of a Ligand in Direct Contact with a Protein Receptor. *J. Am. Chem. Soc.* **2001**, *123*, 6108-6117.

[107] ''Becke's three parameter hybrid method using the LYP correlation functional'' Axel D., Becke J. *Chem. Phys.* **1993,** *98*, 5648.

[108] ''AMBER 12'' D.A. Case, T.A. Darden, T.E. Cheatham, III, C.L. Simmerling, J. Wang, R.E. Duke, R. Luo, R.C. Walker, W. Zhang, K.M. Merz, B. Roberts, S. Hayik, A. Roitberg, G. Seabra, J. Swails,A.W. Götz, I. Kolossváry, K.F.Wong, F. Paesani, J. Vanicek, R.M.Wolf, J. Liu, X. Wu, S.R. Brozell, T. Steinbrecher, H. Gohlke, Q. Cai, X. Ye, J. Wang, M.-J. Hsieh, G. Cui, D.R. Roe, D.H. Mathews, M.G. Seetin, R. Salomon-Ferrer, C. Sagui, V. Babin, T. Luchko, S. Gusarov, A. Kovalenko, and P.A. Kollman (**2012**), University of California, San Francisco.

[109] ''AMBER 2016'' Case D.A., Betz R.M., Cerutti D.S., Cheatham T.E., III, Darden T.A., Duke R.E., Giese T.J., Gohlke H., Goetz A.W., Homeyer N., Izadi S., Janowski P., Kaus J., Kovalenko A., Lee T.S., LeGrand S., Li P., Lin C., Luchko T., Luo R., Madej B., Mermelstein D., Merz K.M., Monard G., Nguyen H., Nguyen H.T., Omelyan I., Onufriev A., Roe D.R., Roitberg A., Sagui C., Simmerling C.L., Botello-Smith W.M., Swails J., Walker R.C., Wang J., Wolf R.M., Wu X., Xiao L. and Kollman P.A. **2016**, University of California, San Francisco.

[110] '' GLYCAM06: A generalizable biomolecular force field. Carbohydrates'' Kirschner K. N., Yongye A. B., Tschampel S. M., Gonzalez-Outeirino J., Daniels C. R., Foley B. L., Woods R. J. *J Comput Chem* **2008,** *29* (4), 622-55.

[111] ''AMBER 9 program'' Wang J., Wolf R. M., Caldwell J. W., Kollman P. A., Case D. A. *J Comput Chem* **2004,** *25* (9), 1157-74.

[112] ''Fast, efficient generation of high-quality atomic charges. AM1-BCC model: II. Parameterization and validation'' Jakalian A., Jack D. B., Bayly C. I. *J Comput Chem* **2002,** *23* (16), 1623-41.

[113] ''Settle: An analytical version of the SHAKE and RATTLE algorithm for rigid water models'' Miyamoto S., Kollman P. A. *Journal of Computational Chemistry* **1992,** *13* (8), 952-962.

[114] '' Particle mesh Ewald: An N·log(N) method for Ewald sums in large systems'' Darden T., York D., Pedersen L. *The Journal of Chemical Physics* **1993,** *98* (12), 10089-10092.

[115] ''A smooth particle mesh Ewald method'' Essmann U., Perera L., Berkowitz M. L., Darden T., Lee H., Pedersen L. G. *The Journal of Chemical Physics* **1995,** *103* (19), 8577-8593.

[116] ''Adventures in improving the scaling and accuracy of a parallel molecular dynamics program'' Crowley M., Darden T., Cheatham I.T., Deerfield I.D. *J. Supercomput.* **1997,** *11* (3), 255-278.

[117] ''SPFP: Speed without compromise—A mixed precision model for GPU accelerated molecular dynamics simulations'' Le Grand S., Götz A. W., Walker R. C. *Computer Physics Communications* **2013,** *184* (2), 374-380.

[118] ''Routine access to millisecond time scale events with accelerated molecular dynamics'' Götz A. W., Williamson M. J., Xu D., Poole D., Le Grand S., Walker R. C. *Journal of Chemical Theory and Computation* **2012,** *8* (5), 1542-1555.

[119] ''Routine microsecond molecular dynamics simulations with AMBER on GPUs. 2. Explicit solvent particle mesh Ewald'' Salomon-Ferrer R., Götz A. W., Poole D., Le Grand S., Walker R. C. *Journal of Chemical Theory and Computation* **2013,** *9* (9), 3878-3888.

[120] ''Long-term outcomes of group B streptococcal meningitis'' Libster R., Edwards K.M., Levent F., et al *Pediatrics* **2012**, 130(1): 8–15.
[121] ''Group B streptococcal disease in infants aged younger than 3 months: systematic review and meta-analysis'' Edmond K.M., Kortsalioudaki C., Scott S., et al. *Lancet* **2012**, 379(9815): 547–556.
[122] ''Dynamics of Streptococcus agalactiae colonization in women during and after pregnancy and in their infants'' Hansen S.M., Uldbjerg N., Kilian M., Sorensen U.B. *J Clin Microbiol* **2004**; 42:83-9.

[123] ''Group B Streptococcus vaccine development: present status and future considerations, with emphasis on perspectives for low and middle income countries'' Kobayashi M., Vekemans J., Baker C.J., Ratner A.J., Le Doare K., Schrag S.J. *F1000Research* **2016**; 5:2355.

[124] ''Neonatal group B streptococcal disease: from pathogenesis to preventive strategies'' Melin P. *Clin Microbiol Infect.* **2011**; 17(9): 1294–1303.

[125] ''An overview of global GBS epidemiology'' Le Doare K., Heath P.T. *Vaccine* **2013**; 31(Suppl 4): 7–12.

[126] ''Molecular pathogenesis of neonatal group B streptococcal infection: no longer in its infancy'' Doran K.S., Nizet V. *Mol Microbiol.* **2004**; 54:23-31.

[127] ''Perinatal group B streptococcal infections across intact amniotic membranes'' Katz V., Bowes W.A. Jr. J *Reprod Med.* **1988**; 33(5): 445–449.

[128] ''Group B streptococcal disease in infants: progress in prevention and continued challenges'' Verani J.R., Schrag S.J. *Clin Perinatol.* **2010**; 37(2): 375–392.

[129] ''Perinatal infections due to group B streptococci'' Gibbs R.S., Schrag S., Schuchat A. *Obstet Gynecol*. **2004**; 104(5 Pt 1): 1062–1076.

[130] ''The natural history of group B streptococcal colonization in the pregnant woman and her offspring'' Yow M.D., Leeds L.J., Thompson P.K., et al. *Am J Obstet Gynecol*. **1980**; 137(1): 34–38.

[131] ''Disease Burden of Group B Streptococcus Among Infants in Sub-Saharan Africa: A Systematic Literature Review and Meta-Analysis'' Sinha A., Russell L.B., Tomczyk S., et al. *Pediatr Infect Dis J*. **2016**; 35(9): 933–42.

[132] ''Prevalence of maternal colonization with group B streptococcus: a systematic review and meta-analysis'' Kwatra G., Cunnington M.C., Merrall E., et al. *Lancet Infect Dis*. **2016**; 16(9): 1076–1084.

[133] ''Prevention of early-onset neonatal group B streptococcal disease with selective intrapartum chemoprophylaxis'' Boyer K.M., Gotoff S.P. *N Engl J Med.* **1986**; 314(26): 1665–1669.

[134] ''Group B streptococcus (GBS) and neonatal infections: the case for intrapartum chemoprophylaxis'' Garland S.M., Fliegner J.R. *Aust N Z J Obstet Gynaecol.* **1991**; 31(2): 119–122.

[135] ''Altering the intestinal microbiota during a critical developmental window has lasting metabolic consequences'' Cox L.M., Yamanishi S., Sohn J., et al. *Cell.* **2014**; 158(4): 705–721.

[136] ''IgG placental transfer in healthy and pathological pregnancies'' Palmeira P., Quinello C., Silveira-Lessa A.L., et al. *Clin Dev Immunol*. **2012**; 2012: 985646.

[137] ''Immunization of pregnant women with group B streptococcal type III capsular polysaccharide-tetanus toxoid conjugate vaccine'' Baker C.J., Rench M.A., McInnes P. *Vaccine* **2003**; 21(24): 3468–3472.

[138] ''Relevance of age at diagnosis to prevention of late-onset group B streptococcal disease by maternal immunization'' Edwards M.S., Rench M.A., Baker C.J. *Pediatr Infect Dis J*. **2015**; 34(5): 538–539.

[139] ''A maternal vaccine against group B Streptococcus: past, present, and future'' Chen V.L, Avci F.Y., Kasper D.L. *Vaccine* **2013**; 31(Suppl 4): 13–19.

[140] ''Status of group B Streptococcal vaccine development'' Lin S.M., Zhi Y. et al. *Clin Exp Vaccine Res* **2018**; 7:76-81.

[141] ''Antibody kinetics and response to routine vaccinations in infants born to women who received an investigational trivalent group B streptococcus polysaccharide CRM197-conjugate vaccine during pregnancy'' Madhi S.A., Koen A., Cutland C.L., et al. *Clin Infect Dis* **2017**; 65:1897-904.

[142] ''Structural elucidation of Type III group B *Streptococcus* capsular polysaccharide using molecular dynamics simulations: the role of sialic acid'', González-Outeiriño J., Kadirvelraj R., Woods R. J. *Carbohydrate Research* **2005**, 340, 1007-1018.

[143] ''Conformation and Cross-Protection in Group B Streptococcus Serotype III and Streptococcus pneumoniae Serotype 14: A Molecular Modeling Study'', <u>Kuttel</u> M. M. and <u>Ravenscroft</u> N. *Pharmaceuticals* **2019**, *12*(1), 28.

[144] ''Structure of a protective epitope of Group B Streptococcus type III capsular polysaccharide'' Carboni F., Adamo R., Fabbrini M., De Ricco R., Cattaneo V., Brogioni B., Veggi D., Pinto V., Passalacqua I., Oldrini D., Rappuoli R., Malito E., Margarit I. and Berti F. *PNAS* **2017**; 114(19):5017-5022.